JOURNAL OF GEOPHYSICAL RESEARCH, VOL. 101, NO. D6, PAGES 9621–9656, APRIL 30, 1996

Comparison of correlative data with HNO_3 version 7 from the CLAES instrument deployed on the NASA Upper Atmosphere Research Satellite

J. B. Kumer,[1] J. L. Mergenthaler,[1] A. E. Roche,[1] R. W. Nightingale,[1] G. A. Ely,[1] W. G. Uplinger,[1] J. C. Gille,[2] S. T. Massie,[2] P. L. Bailey,[2] M. R. Gunson,[3] M. C. Abrams,[3] G. C. Toon,[3] B. Sen,[3] J.-F. Blavier,[3] R. A. Stachnik,[3] C. R. Webster,[3] R. D. May,[3] D. G. Murcray,[4] F. J. Murcray,[4] A. Goldman,[4] W. A. Traub,[5] K. W. Jucks,[5] and D. G. Johnson[5]

Abstract. The cryogenic limb array etalon spectrometer (CLAES) aboard UARS made near-global measurements of HNO_3 and 388 days from January 9, 1992, to April 25, 1993, have been processed to data version 7 (V7). Results from UARS instruments, including CLAES, the improved stratospheric and mesospheric sounder, and the microwave limb sounder, provide the first near-global documentation of the evolution of denitrification in the Antarctic 1992 winter and spring vortex. We provide a description of the CLAES HNO_3 V7 quality that includes comparisons with correlative measurements to assess overall quality, accuracy, and precision. Correlative profiles of volume mixing ratio (vmr) included those obtained by the space shuttle deployed ATMOS in two missions, March-April 1992 and April 1993, data from a variety of balloon-borne instruments at midlatitude (11 profiles), and in high-latitude northern winter (six profiles), and LIMS data. In general, the CLAES V7 HNO_3 maximum values of vmr were of the order of 6–15% less than correlative for CLAES values $\leq$8 parts per billion by volume (ppbv). However, when CLAES peak vmr values were 10 to 13 ppbv, then CLAES values exceeded correlative by 0–7%. The comparisons were within the combined instrumental error estimates, or observed measurement variability, for the large majority of comparisons. As discussed, the retrieval of future versions will utilize updated spectral parameters and will also correct for a small uncompensated drift in radiometric calibration that occurred in the latter part of the mission. This is expected to improve the comparisons in the $\leq$8 ppbv range, perhaps at the expense of those in the $\geq$8 ppbv range. The data obtained January 9 to April 15, 1992, in comparison with data obtained January 9 to April 15, 1993, reveal strikingly evident 1-year period deseasonalized trends on a global basis. These trends agree quantitatively with available correlative data suitable for trend analysis. These include ATMOS in the southern midlatitudes and published long-term time series of HNO_3 column obtained at 45°S and 20°N. These trends reveal a large decrease in the southern hemisphere and small increases in the northern hemisphere, such that the global average is toward a decrease. The global average decrease we attribute to the diminishing influence of heterogeneous conversion of N_2O_5 to HNO_3 as the Pinatubo aerosol settles out during this time period, and the HNO_3 recovers toward pre-Pinatubo conditions. We establish plausibility that the small increases in the north are due to hemispherically asymmetric QBO-like effects that are strong in the northern hemisphere and weak in the southern hemisphere and are phased to produce an increase in HNO_3 over the 1-year time period of just the right magnitude to more than offset decrease due to settling out of the Pinatubo aerosol. Based on this study, our range of confidence in the CLAES HNO_3 V7 product is from 70 to 3 mbar, in comparison with correlative data, and the precision on this range is of the order of 0.3–1.0 ppbv. This precision was derived from data repeatability and agrees within a factor of 2 or better with estimates based on instrument characterization and with error estimates embedded within the V7 data.

[1]Lockheed Palo Alto Research Laboratory, Palo Alto, California.
[2]National Center for Atmospheric Research, Boulder, Colorado.
[3]Jet Propulsion Laboratory, Pasadena, California.
[4]University of Denver, Denver, Colorado.
[5]Smithsonian Astrophysical Observatory, Cambridge, Massachusetts.

Paper number 95JD03759.
0148-0227/96/95JD-03759$05.00

1. Introduction

As discussed by various authors, measurement of stratospheric HNO_3 is interesting with regard to three different aspects of the problem of O_3 destruction in the middle stratosphere. First, on a global scale it is the product of the reaction $OH + NO_2 + M \rightarrow HNO_3 + M$ which is important in disrupting the major catalytic cycle for O_3 destruction, namely, the odd nitrogen catalytic cycle involving NO and NO_2. The resultant HNO_3 is a relatively nonreactive form of odd nitrogen that is transported down to the troposphere where it is rained out, the principal sink mechanism for stratospheric odd nitrogen. Second, in the extremely cold Antarctic winter-spring, HNO_3 is depleted by condensation on to aerosols and sedimentation. This leads to depletion in NO_2 since it is produced mainly by $h\nu + HNO_3 \rightarrow OH + NO_2$. Relatively large amounts of active Cl then can exist in the atmosphere since there is not enough NO_2 to effectively remove it by $NO_2 + ClO + M \rightarrow ClONO_2 + M$. The end result is dramatic reduction of ozone due to the Cl catalytic cycle. Third, in the presence of enhanced stratospheric sulphate aerosol as was produced by the Pinatubo eruption, reactions on the aerosol surface can convert N_2O_5 to HNO_3 and significantly reduce the odd nitrogen in the atmosphere [*Hoffman and Solomon*, 1989], leading to enhanced ozone reduction due to corresponding increases in active chlorine and odd hydrogen that are suppressed by active nitrogen. Finally, a long-term global data set makes it possible to look for the relatively large effects of the quasi-biennial oscillation (QBO) on HNO_3 that have been predicted by various authors [*Chipperfield and Gray*, 1992; *Gray and Ruth*, 1992].

There are three instruments deployed on the UARS that address HNO_3 measurement, CLAES, ISAMS, and MLS. These instruments also measure many other important chemical constituents of the upper atmosphere, as described by [*Roche et al.*, 1993a; *Taylor et al.*, 1993; *Waters*, 1993]. These UARS-borne instruments are capable of achieving a high areal coverage density, typically more than 1200 HNO_3 vmr profiles per day for CLAES, for example.

There exist many (too numerous to cite all) single-profile and in situ measurements of HNO_3. Some of the earlier of these are *Murcray et al.* [1968], *Lazrus and Gandrud* [1974], *Fontanella et al.* [1975], *Murcray et al.* [1975], and *Evans et al.* [1976], for example. However, prior to UARS the LIMS [*Gille et al.*, 1984] constituted the only high areal density, nearly global HNO_3 data set. The LIMS data were obtained in the latitude range from 64°S to 84°N and on the time period October 24, 1978, to May 28, 1979. Therefore south polar processes were not observed. In addition to LIMS, space-based solar occultation HNO_3 measurements have been obtained by the ATMOS instrument in shuttle-deployed missions [*Farmer*, 1987; *Farmer et al.*, 1987; *Russell et al.*, 1988], but due to short duration and the relatively limited shuttle mission time periods, these data are generally limited to lower than polar latitudes and considerably lower coverage density than the UARS data. However, due to recent awareness of the south polar ozone depletion [*Farman et al.*, 1985] a number of polar measurement campaigns, including the Airborne Antarctic Ozone Experiment (AAOE) in 1987 [*Tuck et al.*, 1989], the Airborne Arctic Stratosphere Expedition (AASE I) in 1989 [*Turco et al.*, 1990] and the AASE II in 1991/1992 [*Rodriguez*, 1993; *Traub et al.*, 1994a, b], have been conducted. These resulted in measurements of HNO_3 at point locations and on aircraft flight profiles that have produced a valuable database on the phenomenology of HNO_3 during heterogeneous ozone depletion events, including its dramatic depletion due to freeze-out and sedimentation during south polar winter. The UARS HNO_3 measurements build on these data by providing high-density global coverage over an extended time period [*Reber*, 1993].

This paper focuses on the 388 days of CLAES data that are processed to V7. These days are interspersed on the period from January 9, 1992, to April 25, 1993. As described by *Roche et al.* [1994], the CLAES is mounted on the cold Sun-shaded side of the UARS which, due to orbital precession, is yawed 180° every ≈36 days to maintain the Sun-shaded condition. Before, during, and after the yaw around maneuver, for a total of approximately 5 days, the telescope door is closed to prevent solar heat load on the cryogen and solar damage to the instrument, and no atmospheric data are obtained in this period. Thus data are obtained for alternate 31-day periods preferentially in the southern or the northern hemisphere, dependent on yaw direction. Viewing north provides global coverage between 80°N and 34°S, and this covers 77% of the Earths' area, and viewing south between 80°S and 34°N. The two viewing directions taken together provide coverage of more than 98% of the globe. Each latitude circle is sampled 30 times per day within these latitude bands, and both illuminated and dark (including polar night) coverage is obtained. Coverage is always obtained in the overlap band between 34°N and 34°S. The orbit precession provides coverage of all local times in the 36-day period. The CLAES measurements cover a variety of atmospheric conditions which include the Arctic and Antarctic winters and the period of heavy stratospheric aerosol loading that resulted from the Mount Pinatubo eruption of June 15, 1991, and the changing conditions as the aerosol settled out of the atmosphere. CLAES HNO_3 observations have been previously published by *Roche et al.* [1993b] for selected days in the 1992 south polar winter, and *Roche et al.* [1994] expands on that with an overview of the observed morphological and seasonal behavior of HNO_3 in both hemispheres over the V7 processing time period with emphasis on the high-latitude lower-stratospheric region of prime interest for heterogeneously driven ozone depletion. This [*Roche et al.*, 1994] paper points out the evolution of the major depletion in south polar HNO_3 in the winter and spring that is clearly evident in the CLAES data. The CLAES instrument was able to obtain these observations in consecutive south-looking periods spanning the event. The *Roche et al.* [1994] paper also addresses comparisons of CLAES V7 HNO_3 with the Lawrence Livermore National Laboratory heterogeneous chemistry model; therefore this paper will not address model comparisons.

This paper supports and builds on the previous CLAES HNO_3 publications. It provides a description of the V7 data characteristics that is required for appropriate use of these data by the community. In developing this description, on comparing data within the period January 9 through April 15, 1992, with corresponding data within the period January 9 through April 15, 1993, it became clear that strikingly obvious 1-year deseasonalized trends are globally present in the data. Where correlative data are available to check these trends, they agree quantitatively. This includes the ATMOS data obtained in the southern hemisphere in late March-early April 1992 and in early April 1993, HNO_3 column times series data at 45°S [*Koike et al.*, 1994], and at 20°N [*David et al.*, 1994]. A more detailed description of the trends is given in sections 3.2 and 5.1 below, and a discussion of mechanisms is provided in

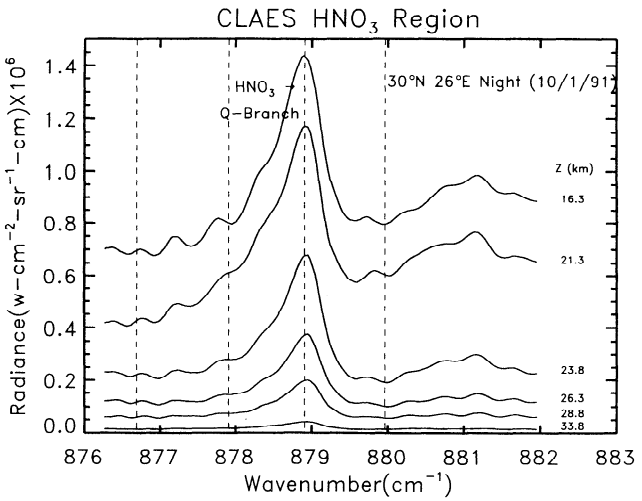

Figure 1. Cryogenic limb array etalon spectrometer (CLAES) continuous spectra obtained in blocker region 6, targeted for HNO_3 retrieval.

section 5.2. The remainder of this paper is divided into five sections. The first (section 2) provides a brief review of the instrument and measurement technique and the V7 approach for retrieval and computation of the error estimates that are embedded in the reported V7 data. Section 3 presents the comparisons with correlative data and analyses to establish estimates of systematic error and precision. In section 4, systematic and random error estimates that are based on instrument characterization are derived and compared with results obtained from comparisons with correlative measurements. In section 5 the trends are described in more detail and compared with correlative data, trend mechanisms are discussed, and data usage caveats are presented. The final section 6 presents a summary and conclusion.

2. Methodology

The CLAES derives geophysical quantities from infrared radiance emissions in a limb-viewing mode. Nine spectral regions are sequentially isolated to retrieve pressure, temperature, HCl, NO, H_2O, NO_2, N_2O_5, CH_4, N_2O, CFC-12, CFC-11, HNO_3, O_3, and $ClONO_2$. The CLAES optical system and measurement technique are described by *Roche et al.* [1993a]. In brief, after entering the instrument through a telescope designed to minimize stray light, the Earth-limb thermal emission passes through one of four Fabry-Perot etalons which are mounted in a paddle wheel and one of nine order blocking filters mounted in a filter wheel. Each filter isolates a narrow spectral region that includes spectral features of one or more target species. The CLAES filters actual performance for $\Delta\nu/\nu$ ranged from 0.4 to 0.7% where ν refers to the spectral center of the filter passband and where $\Delta\nu$ refers to the filter passband full width at half maximum. The Fabry-Perot provides spectral resolution of the order of 20 to 30 times better than that of the filter, within the filter passband. Thus resolutions of the order of 0.2 cm^{-1} are achieved at the longest wavelength region near 780 cm^{-1} and of the order 0.65 cm^{-1} in the region near 2843 cm^{-1}. The etalon is tilt tuned within a filter passband by means of tilting the paddle wheel. A tilt through a nominal range of 20° to 25° provides a complete spectral scan at etalon resolution within the filter passband. Aspects of the instrument spectral characterization have been described in numerous references by *Roche et al.* [1993a] and by *Mergenthaler et al.* [1990]. The spectrally filtered radiation falls on a focal plane assembly consisting of a main array of 20 elements and an HCl array of 3 elements. The main detector array is used by eight longer-wavelength channels, one of which targets HNO_3, and takes atmospheric data simultaneously in twenty 2.5 km vertical increments giving altitude coverage from approximately 10 to 60 km.

Examples of the continuous spectra obtained simultaneously on several of the 20 CLAES detectors when scanning the etalon in the spectral region near 879 cm^{-1} that was selected for HNO_3 retrieval (i.e., "blocker 6") are shown in Figure 1. The type of spectra shown in Figure 1 require an entire 65-s period to complete the scan through the blocker passband. This is too long to be done on a routine basis because 65 s is the period selected for repetition of the total set of instrument measurements by the UARS science team. The CLAES total measurement set includes much more than HNO_3, so only a small fraction of the 65 s can be spent on obtaining measurements in the HNO_3 region, similar applies for the other CLAES species. For CLAES to obtain an entire measurement set within time limit requires that only a small number of samples can be obtained within each blocker filter passband. These are listed for all CLAES blocker regions by *Roche et al.* [1993a]. By inspection of this list it can be seen that the CLAES retrieval process involves multiple channels and multiple emitters on each blocker region. For the 879 cm^{-1} region there are four measurement channels and two retrieved species, HNO_3 and aerosol, as shown below in Table 1.

The CLAES approach for retrieval and error estimation for V7 data for the CLAES multiemitter multichannel problem is discussed in Appendix A below. The problem is broken down to the equivalent of a single-emitter and single-channel problem for each specie i by using a linear least squares approach for fitting calculated radiances to the observed data. In our case this procedure provides an equivalent single-specie single-channel retrieval problem for HNO_3 and aerosol. Next, a method similar to the Newtonian iterative algorithm [*Rodgers*, 1976, equation (99), p. 621] is used for retrieval and error estimation for each specie i. For production data processing the method requires a computationally efficient algorithm for calculation of radiance profiles. The model described by *Marshall et al.* [1994] is used for this purpose. The method uses "initial guess" species profiles from the UARS prelaunch climatology that was developed (by R. R. Seals and D. J. Wuebbles) for the UARS science team, and a description

Table 1. Narrowband Channels Used in the HNO_3 Region

Spectral Position, cm^{-1}	Spectral Feature and Comment
876.69	local minimum in HNO_3 spectral radiance, optimizes spectral contrast for aerosol retrieval*
877.91	local maximum in HNO_3 spectral radiance
878.91	largest maximum in HNO_3 spectral radiance, occurs at the ν_5 q branch
879.96	local minimum in HNO_3 spectral radiance

*The retrieval procedure is described in more detail in Appendix A. On a fractional basis the aerosol contribution is emphasized in the "HNO_3 local minimum channels," and these were selected for use by CLAES to facilitate its retrieval.

provided by P. S. Connell is given by *Kumer et al.* [1993]. Retrieval of a CLAES species (such as HNO_3) profile requires the use of a pressure and temperature profile. These are the first parameters obtained in the general CLAES retrieval process, and these are retrieved from data obtained in the spectral region centered at 790 cm^{-1}, as is discussed by *Roche et al.* [1993a] and *Gille et al.* [this issue].

Figure 2 shows the initial climatological guess and the results from seven iterations of the retrieval process for a typical HNO_3 and aerosol retrieval. The final solution is much different than the initial guess and the changes between successive iterations decrease rapidly. Four iterations which are used in the V7 software are sufficient to achieve a solution within variance estimates.

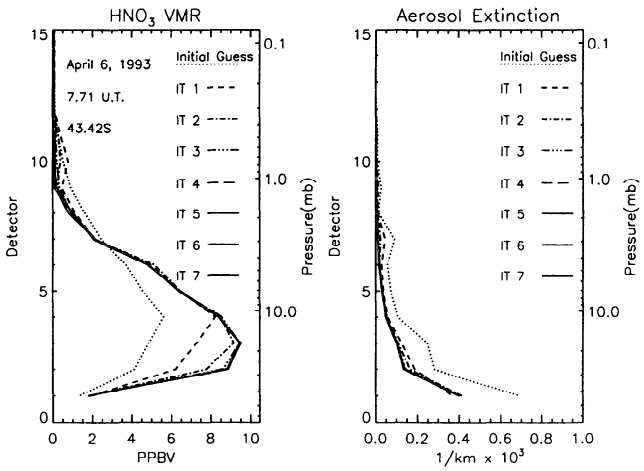

Figure 2. Initial climatological guesses and the results from seven iterations for a typical retrieval of HNO_3 and aerosol profiles.

3. Correlative Comparisons

3.1. Description of Correlative Data Sources

A comprehensive set of correlative measurements are examined to assess the CLAES data quality. A subset of HNO_3 measurements obtained during the mission and the LIMS measurements from before the mission are used. Some HNO_3 measurements that were made during the UARS mission may be omitted from this discussion, but we believe we have included enough data from independent and well-proven sources to provide a solid basis for comparison. The LIMS data are also used as these represent the only available correlative data that can be used to obtain global comparison. The discussion addresses comparisons versus HNO_3 vmr profiles measured from the space-shuttle-borne ATMOS during the Atmospheric Laboratory for Applications and Science (ATLAS) 1 and 2 missions, versus profiles obtained by various balloon-deployed instrumentation during the operational life of the CLAES, and comparisons with LIMS zonal mean cross sections for representative seasonal and regional cases.

The Atmospheric Trace Molecule Spectroscopy (ATMOS) experiment is a shuttle-deployed instrument. It is a fast-scanning high-resolution (0.01 cm^{-1}, unapodized) Michelson interferometer that records solar occultation spectra in the 2- to 16-μm region from Earth orbit. A series of high-resolution spectra of the Sun at tangent height separation of 4 km through and above the atmosphere were recorded at sunrise and sunset. The spectra of transmission through the atmosphere record the absorption of many molecular species, including the correlative species N_2O, CH_4, HNO_3, $CLONO_2$, N_2O_5, and CF_2Cl_2 for comparison with UARS data. A detailed description of the ATMOS experiment and the measurements obtained during the Spacelab 3 shuttle mission has been given by *Farmer* [1987] and *Farmer et al.* [1987]. Measurements of many of these species in the original ATMOS mission on Spacelab 3 have been discussed by *Russell et al.* [1988] and *Gunson et al.* [1990]. During the CLAES lifetime, ATMOS was deployed and gathered correlative data in two shuttle flights, the ATLAS 1 mission in late March and early April 1992 and the ATLAS 2 mission in mid-April 1993.

The far-infrared spectrometer (FIRS-2) instrument is described by *Traub et al.* [1991] and *Johnson et al.* [1995]. It is a high-resolution, far-infrared thermal emission Fourier-transform spectrometer that operates on a balloon-borne platform at about 39 km altitude. It operates in both the far infrared (80–220 cm^{-1}) and the mid-infrared (350–700 cm^{-1}) with an unapodized spectral resolution of 0.004 cm^{-1}. Since FIRS-2 measures thermal emission spectra of molecular rotational and vibrational transitions, it can operate throughout the diurnal cycle. In addition to HNO_3 the FIRS-2 obtained correlative temperature, pressure, HCl, H_2O, O_3, NO_2, and N_2O data for comparison with CLAES data. These data are available for three balloon flights of this instrument launched from Ft. Sumner, New Mexico, on May 29, 1992 (36.5°N, 255.2°E), and on September 29, 1992 (36.9°N, 259.6°E), and from Barstow (Daggett Airport), California, on March 24, 1993 (37.1°N, 252.5°E), and covering the altitude range of 18–40 km. A fourth flight was executed May 22, 1994 but will not be considered in this discussion because this was well after the end of CLAES life.

The balloon-borne laser in situ sensor (BLISS) instrument measurement concept, operational details, and data reduction procedures have been described by *Webster et al.* [1987, 1990, 1994]. It is a high-resolution (0.0001 cm^{-1}) absorption spectrometer in the mid-infrared wavelength region using tunable diode laser (TDL) sources. The instrument probes in situ a region of the stratosphere away from the gondola by sequentially transmitting TDL beams to a retroreflector suspended 200 m below the instrument gondola. Volume mixing ratios of NO_2, CH_4, HNO_3, and HCl have been determined for nighttime conditions for August 26, 1992, near Palestine, Texas (31.4°N, 261.2°E). These were obtained over the altitude range of 23 to 33 km. Because the instrument can only measure one species at a time, approximately three different altitude measurements of each species were accomplished on this flight, considerably farther apart than the intrinsic 0.2-km resolution of the instrument. The predicted minimum detectable mixing ratio at 30 km is typically <0.1 ppbv for many stratospheric constituents of interest. Accuracy of the HNO_3 measurement is ±11%.

The sub-millimeter-wave limb sounder (SLS) instrument is described by *Stachnik et al.* [1992]. It is a balloon-borne sub-millimeter-wave radiometer simultaneously measuring thermal emission spectra from HNO_3, ClO, HCl, O_3, and H_2O in the 600-GHz spectral region. The instrument obtains limb spectra from float altitude, typically 38 km. Stratospheric vmr is obtained for these constituents from 15 to 50 km with a resolution of 3 to 5 km. The accuracy for the HNO_3 measurement is about 20% with an averaging time of 15 min as set by the 25-min duration of one limb scan sequence. HNO_3 data taken on September 29, 1992, from Ft. Sumner, New Mexico (35.5°N,

259.0°E), and on April 3, 1993, from Barstow (Daggett Airport), California (34.5°N, 249.0°E), have been used for comparison with CLAES HNO_3.

The JPL MARK IV (i.e., MkIV) interferometer, described by *Toon* [1991], is a high-resolution solar absorption spectrometer which measures the entire 650 to 5650 cm^{-1} region simultaneously at a resolution of 0.01 cm^{-1}. From balloon the MkIV is capable of obtaining volume mixing ratio vertical profiles between cloud top and balloon altitude (typically 37 km) for a number of UARS species, including HNO_3, CF_2Cl_2, CH_4, N_2O, NO_2, HNO_3, $ClONO_2$, and N_2O_5 and can also obtain total column measurements above the balloon float altitude. Two flights of this instrument on September 14–15, 1992, from Ft. Sumner (34.5°N, 255.7°E) and another on April 4, 1993, from Barstow (Daggett Airport) (34.9°N, 243.2°E) were available for this validation exercise. The earlier flight provided both sunrise and sunset data, the latter just sunset data.

The Bomem Fourier transform spectrometer (FTS) instrument is described by *Murcray et al.* [1990]. It is a modified Bomem model DA3.002 Fourier transform spectrometer (FTS) with a maximum optical path difference of 250 cm, which corresponds to spectral resolution (full width half maximum of the instrument response function) of 0.0024 cm^{-1}. It is used to obtain atmospheric solar absorption spectra. It uses a liquid nitrogen-cooled mercury cadmium telluride (MCT) detector that covered a useful band-pass region from approximately 750 to 1280 cm^{-1}. Analysis of infrared absorption spectra collected during the balloon flight on July 24, 1992, launched from Palestine, Texas (31.6°N, 259.5°E), yielded measurements of HNO_3, $ClONO_2$, and N_2O. The sunset flight out of Barstow (Daggett Airport), California (35.4°N, 253.7°E), on April 7, 1993, provided observations of HNO_3 and $ClONO_2$. Both flights covered the altitude range of about 15 to 40 km.

The cold atmosphere emission spectral radiometer (CAESR) instrument is described by *Murcray et al.* [1994]. It is a small grating spectrometer, operating at liquid He temperature in a small dewar. The unit obtains atmospheric emission spectra in the 7.5- to 12.6-μm wavelength region as it ascends on a balloon. The altitude profile for HNO_3, covering about 10 to 30 km, is obtained by measuring the change in the spectral radiance with altitude in the regions where HNO_3 has spectral features. For the present data, collected above Kiruna, Sweden (67.5°N, 20.2°E), on January 9 and March 5, 12, and 14, 1992, the CAESR rode piggyback on flights sponsored by the European Arctic Stratospheric Ozone Experiment (EASOE).

The Michelson interferometer for passive atmospheric sounding, balloon-borne (MIPAS-B) version instrument is described by *Clarmann et al.* [1993, 1994]. It is a cryogenic Fourier transform spectrometer, which was especially designed to record limb emission spectra for simultaneous measurement of atmospheric trace gases during night and polar winter from stratospheric balloons. This spectrometer is a rapid scanning interferometer using a modified Michelson arrangement, which allows a spectral resolution of 0.04 cm^{-1} (unapodized) to be achieved and spectral regions from 770 to 970 cm^{-1}, as well as from 1170 to 1390 cm^{-1}, to be covered. MIPAS-B flew from Esrange, Sweden (68°N, 21°E), as part of the EASOE on January 13 and the night of March 14–15, 1992, measuring HNO_3 and $ClONO_2$.

The limb infrared monitor of the stratosphere (LIMS) instrument is described by *Gille and Russell*, 1984]. It was a six-channel broadband limb-scanning radiometer that was deployed on Nimbus 7 and obtained data in the latitude range from 64°S to 84°N and on the time period October 24 to May 28, 1978. Measurements of H_2O, NO_2, O_3, HNO_3, and temperature were obtained by the LIMS. The HNO_3 was obtained at ≈2.7 km vertical resolution.

3.2. Comparison Results

3.2.1. Comparison with correlative profiles. During the mission, correlative profiles were obtained by the ATMOS and by balloon-borne instrumentation. The ATLAS 1 and 2 shuttle deployments of ATMOS provided the largest number of profiles for comparison and these will be the addressed first. The profiles obtained by balloon-borne instrumentation clustered into two northern latitude regions: one at midlatitudes near the balloon launching facilities in the Southwest, United States, where data were obtained by the FIRS-2, BLISS, SLS, MkIV, and the Murcray Bomem FTS and the second at high latitude near Kiruna, including CAESR and MIPAS-B.

Comparison with ATMOS: The ATLAS 1 flight took place from March 24 to April 7, 1992, during heavy stratospheric aerosol loading from the Mount Pinatubo eruption of June 15, 1991. The ATMOS HNO_3 data version 1 was used for these comparisons. It is described by M. R. Gunson et al. (manuscript in preparation, 1995). The version 2 will be released in the near future. Coincidence with CLAES data facilitated comparisons with 17 ATMOS sunset occultation profiles in a south midlatitude band and 21 comparisons with ATMOS sunrise profiles in a latitude band ranging from the south tropics to the north subtropics.

Comparison of CLAES and ATMOS profiles are based on coincidence measurements within a criterion of ±2° latitude, ±10° longitude, and ±12 hours. Sometimes, more than one CLAES profile would satisfy these conditions. In these cases, to make single CLAES to ATMOS profile comparisons, the CLAES profile, satisfying the coincidence criteria and also closest in time, was selected. Representative examples of these are shown in Figure 3. The vertical scale in Figure 3 is labeled both by the pressure and by the equivalent coordinate z, a function of pressure that approximates altitude; that is, $z \equiv (3 - \log_{10}(p)) \times 16$ km, where p is pressure in millibars. The coordinate z rather than p is usually used for registration comparisons between CLAES and correlative measurements in this paper. The examples in Figure 3 were selected to illustrate some of the better and worse comparisons with ATMOS and also to facilitate discussion below that is related to trends that are observed in the south midlatitude from April 1992 to April 1993. These 17 single-profile coincidences occurred on a latitude band ranging from 31.8°S to 55.5°S with mean value 47.9°S and $\sigma \approx 5.6°$. For these 17 profiles the average value for the altitude where the peak vmr occurred in the ATMOS and CLAES profiles was 25.0 ± 1.2, and 24.6 ± 1.0 km, respectively. The average value for the peak vmr in the ATMOS and CLAES profiles was 9.55 ± 0.7 and 10.25 ± 1.3 ppbv, respectively. Some of the variability in the peak vmr of each occurs due to the variation of the profiles with latitude. The variability of the difference in peak volume mixing ratios removes latitudinal variation and is 1.02 ppbv, i.e., 11%.

A statistical comparison presenting the mean value of the normalized difference (CLAES-ATMOS)/CLAES and the standard deviations of this quantity, which can be interpreted as a range of variability, are shown in Figure 4a. These statistics were derived from all profiles that satisfied the coincidence criteria above, not just those closest in time. Since the altitude

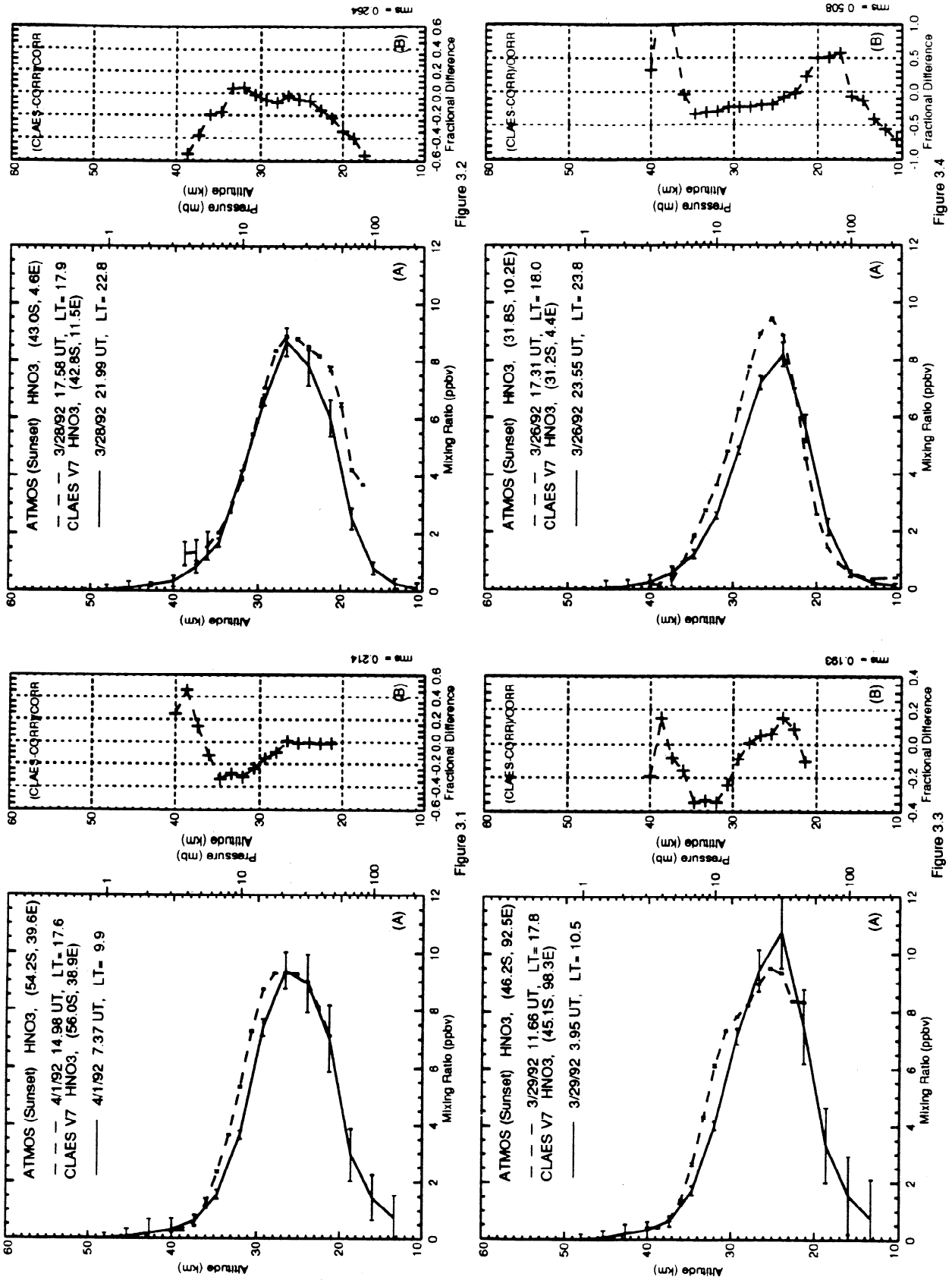

Figure 3.3 Figure 3.4 Figure 3.2 Figure 3.1

Figure 3. Eight representative profile comparisons of CLAES versus ATMOS for the 1992 sunset ATMOS profiles obtained from March 26 to April 2.

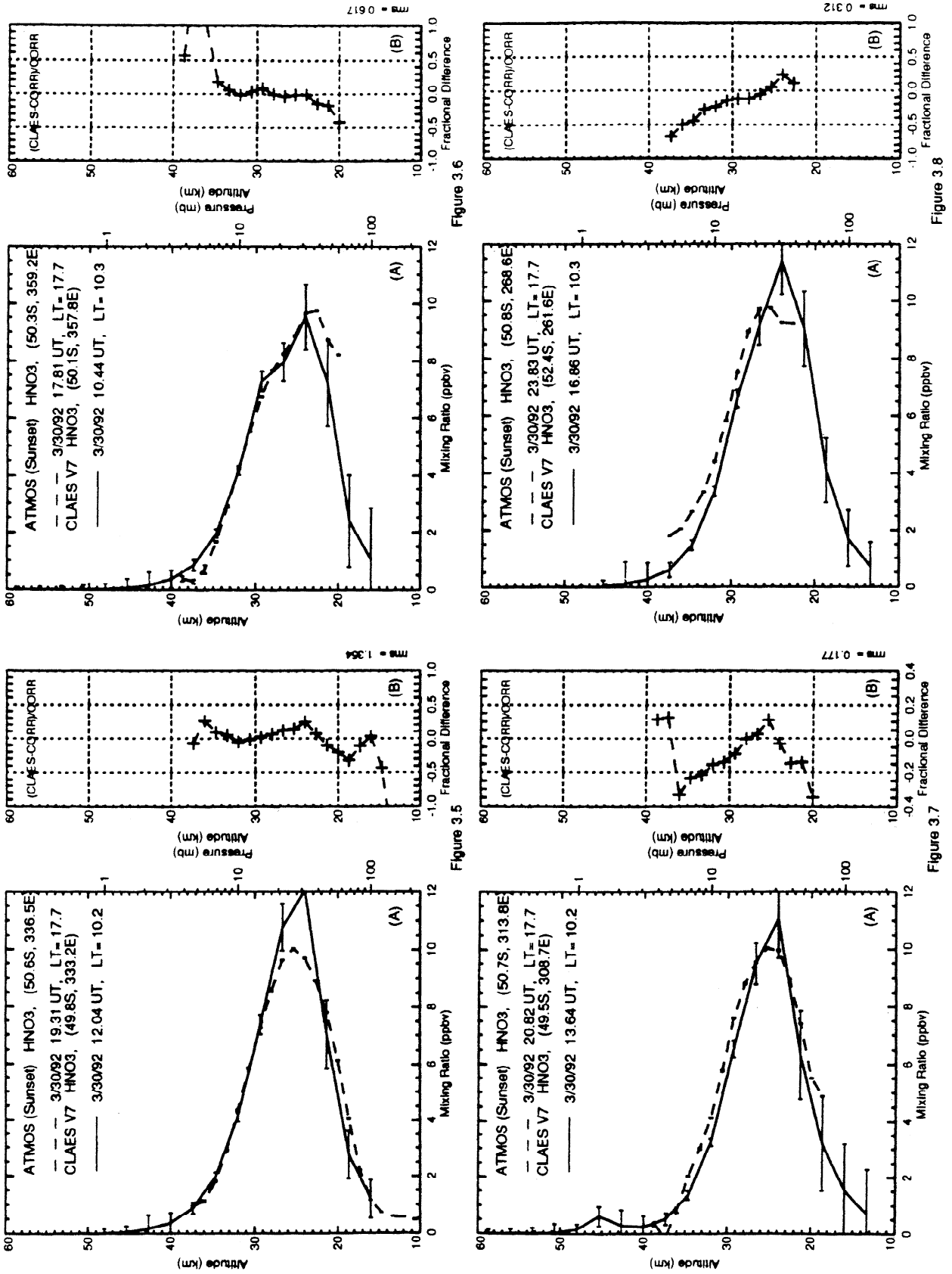

Figure 3.6 Figure 3.8

Figure 3.5 Figure 3.7

Figure 3. (continued)

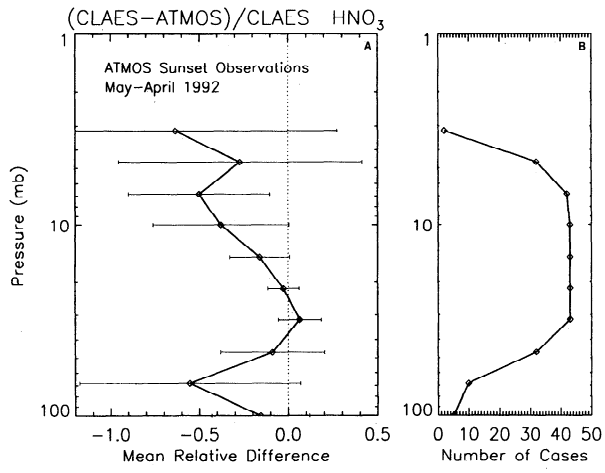

Figure 4. (a) Mean value of the normalized difference (CLAES-ATMOS)/CLAES and the standard deviations of this quantity for the 1992 ATMOS sunset data. (b) Number of coincident points that contribute to the statistics shown in Figure 4a at each pressure level.

range of overlap can be quite different for CLAES and ATMOS profiles, the number of coincident points that contribute to the statistics at each pressure level can differ; these are plotted in Figure 4b. Registration, vmr value at peak, and the width of the profile all affect the statistics shown in Figure 4. Because of ATMOS data sparsity the low-altitude (70 mbar and greater) comparisons are less meaningful. The agreement is essentially within the range of variability for all points at higher altitude, except at 7 mbar where the CLAES is less than ATMOS and slightly outside the range of variability.

The ATMOS-ATLAS 1 tropical sunrise data are limited in altitude coverage since the Pinatubo aerosol prevented the near-infrared Sun sensor from acquiring the rising Sun at altitudes below about 27 km. Figure 5 shows four representative examples from 21 single-profile comparisons of CLAES to ATMOS sunrise in the tropics. Sixteen of these ATMOS profiles extended to low enough altitudes to include the altitude where the peak value of the vmr occurs. These 16 profiles occurred on the latitude range from 16.7°S to 18.2°N, with mean latitude 3.0°N and $\sigma \approx 9.8°$. For these 16 profiles the average value for the altitude where the peak vmr occurred in the ATMOS and CLAES profiles was 29.7 ± 1.0 and 29.1 ± 2.0 km, respectively. The average value for the peak vmr in the ATMOS and CLAES profiles was 4.9 ± 0.7 and 4.2 ± 0.6 ppbv, respectively. The variability of the difference in peak volume mixing ratios is 0.50 ppbv, i.e., 12%.

A statistical comparison of relative mean differences and standard deviations of CLAES data with the ATMOS 92 sunrise data is shown in Figure 6a. These were derived in a manner similar to those shown in Figure 4a, and Figure 6b likewise shows the points from multicoincidences that are contributing to these statistics at each pressure level. As discussed above, registration, vmr value at peak, and the width of the profile all affect the statistics shown in Figure 6. The low-altitude data are more sparse than for the sunset case and the data are less meaningful for low altitudes beginning at about 30 mbar. The agreement is essentially within variability for altitudes above 10 mbar, and CLAES is less than ATMOS by slightly more than the variability at the 10- and 14-mbar levels.

The ATLAS 2 flight took place from April 8 to 16, 1993, during a time when the stratospheric aerosol loading from the Mount Pinatubo eruption was significantly dissipated by comparison with the time the ATLAS 1 data were obtained. No sunrise events were obtained coincident with CLAES in this time period because the UARS cold side instruments were looking to the south and the sunrise ATMOS observations were obtained north of 34°N. Using the same coincidence criteria as described above provides 14 individual CLAES versus ATMOS sunset comparisons. These 14 comparisons were obtained in a southern midlatitude band ranging from 27.4°S to 49.5°S with mean latitude 42.3°S and $\sigma \approx 6.8°$. There were fewer sunset profiles obtained by the ATLAS 2 than by the ATLAS 1 mission, and these generally were obtained over a limited altitude range, such that only six of the ATLAS 2 profiles extended down to altitudes low enough to include the peak HNO_3 vmr. Representative examples are shown in Figure 7. Considering those six comparisons, the average value for the altitude where the peak vmr occurred in the ATMOS and CLAES profiles was 25.6 ± 1.4 and 24.7 ± 1.3 km, respectively. The average value for the peak vmr in the ATMOS and CLAES profiles was 5.8 ± 1.5 and 5.4 ± 1.6 ppbv, respectively. The variability of the difference in peak volume mixing ratios is 0.25 ppbv, i.e., 5%.

As described above, a multiple profile statistical comparison of relative mean differences and standard deviations of CLAES data with the ATMOS 93 sunset data is shown in Figure 8. It is interesting to compare these with the ATMOS 92 sunset obtained in nearly the same latitude band one year previous. Compared to ATMOS 92 sunset, the ATMOS 93 sunset data are relatively sparse from 20 mbar on down in altitude. Therefore these data may not be so statistically meaningful through the region of the peak vmr values, i.e., 20 to 40 mbar, as are the ATMOS 92 data. On this range the CLAES data are of the order of 10 to 15% less than the ATMOS 93 sunset data, where as on the average, the CLAES data are about the same as the ATMOS 92 sunset data on this range. Below 40 mbar, variability becomes quite large in both cases. Above 20 mbar the comparison is close to similar for both years, with the agreement a little better for the 1992 case.

Inspection of CLAES zonal mean data suggests a decrease of a factor 1.39 in HNO_3 vmr near the altitude of the peak vmr in south midlatitudes (40° to 50°S) in March/April 1993 as compared with March/April 1992. The question as to whether this is real or an artifact is brought to mind. The ATMOS sunset data can be used to examine this question. The comparison is sparse because there were only six ATMOS profiles going to low enough altitudes to include the peak vmr in 1993, and most of these were obtained in latitude regions closer to the equator than those obtained in 1992. However, there was one ATMOS 93 profile obtained at 50.0°S. On comparing this with four ATMOS 92 profiles obtained at 50.3°, 50.6°, 50.7°, and 50.8°S, we see an average decrease in peak vmr of a factor that is approximately (9.8/7.3 ppbv) = 1.34 in ATMOS data near 50°S on going from 1992 to 1993. In the corresponding comparison of CLAES profiles near 50°S, decrease is a factor of about (11.0/7.4 ppbv) = 1.48. Likewise, there is one ATMOS 92 profile available for 31.8°S, which can be compared with ATMOS 93 profiles at 30.4°, 31.4°, and 32.8°S. For this comparison near 31°S we see an average decrease in peak vmr of about (9.5/6.6 ppbv) = 1.44 in ATMOS data on going from 1992 to 1993, and for the comparison of corresponding CLAES profiles a decrease of about (8.1/6.0 ppbv) = a factor of 1.35. These results suggest there may be a strong 1992 to 1993 trend for decrease in the HNO_3 in these latitude regions.

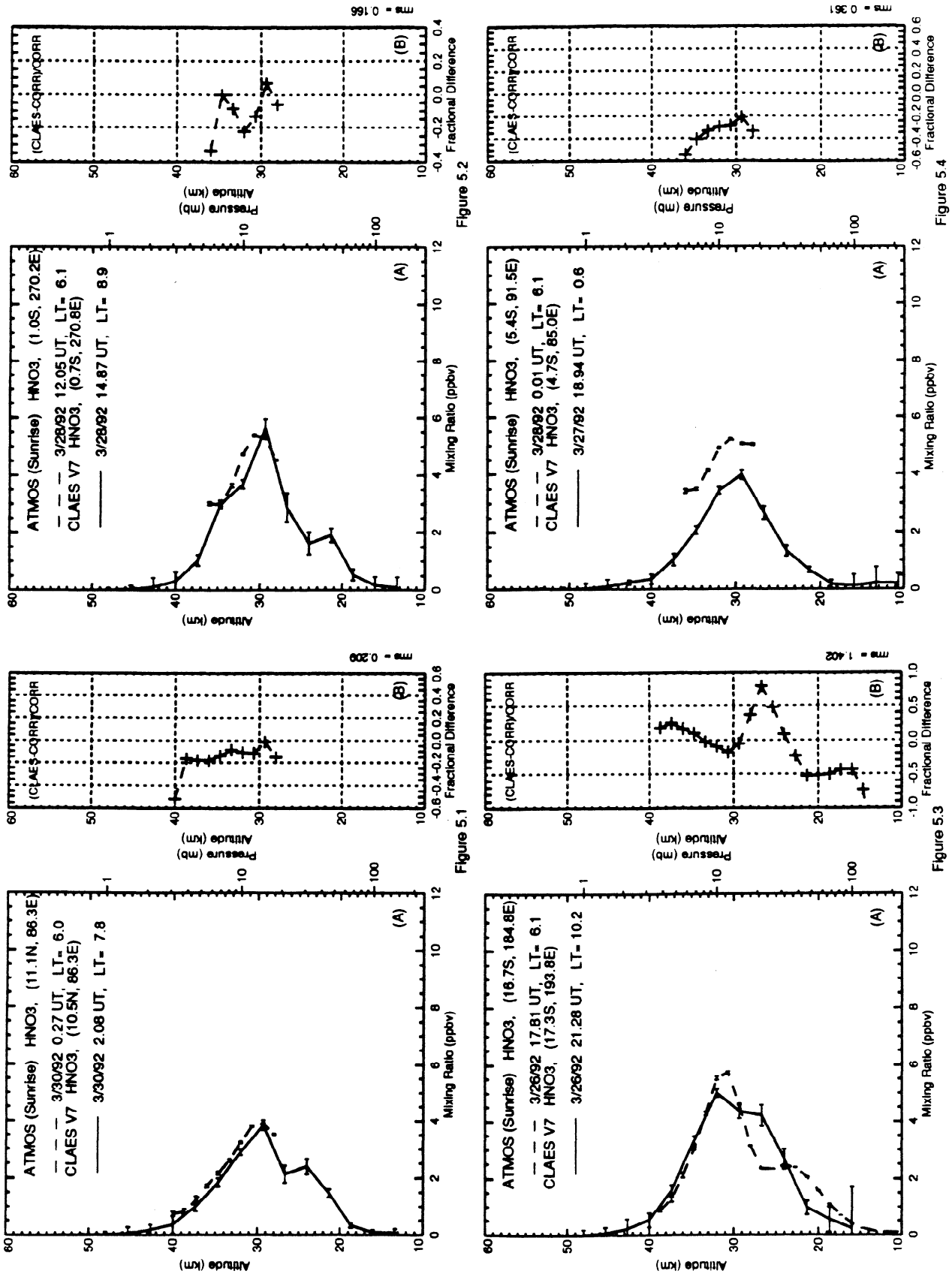

Figure 5.2 Figure 5.4 Figure 5.1 Figure 5.3

Figure 5. Four representative profile comparisons of CLAES to 1992 ATMOS sunrise data in the tropics.

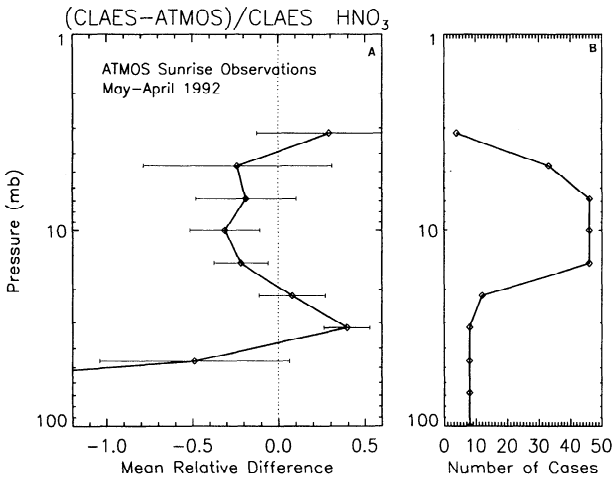

Figure 6. As in Figure 4 but for the 1992 ATMOS sunrise data.

This will be discussed in more detail in section 5.1.1 below. This discussion will generally argue that a real trend is present at these latitudes but that the trend in the CLAES V7 is about 5% smaller than the numbers derived here.

Comparison with midlatitude profiles measured by balloon-borne instrumentation: Comparisons of CLAES data with the FIRS-2 data are presented in Figure 9 for May 29 and September 29, 1992, and March 24, 1993. In general, the three days of comparisons are consistent with one another, with best agreement near peak vmr attained for the September 29, 1992, case. The CLAES profiles are within 2° latitude, 6° longitude, and within 6 hours of the mean time reported for the FIRS-2 data. Considering the three comparison days, for the comparison at altitudes below the peak vmr, the CLAES values are less than the FIRS-2 values, and error estimates overlap except for the March 24, 1993, case. Considering the altitude region near the peak vmr, good agreement is observed for the September 29, 1992, case, but the CLAES data are less than the FIRS-2 by approximately 20% for the other two cases, which is outside the error bar limits. The FIRS-2 data point near 33 mbar exceeds the CLAES value there by approximately 1.7 ppbv for the May 29, 1992, case, and the FIRS-2 data point near 36 mbar exceeds the CLAES value there by approximately 1.5 ppbv for the March 24, 1993, case. The peak values vmr decrease by 18 and 13%, respectively, from May 29, 1992, to March 24, 1993, for CLAES and FIRS-2. On the top side the FIRS-2 values are consistently larger than the CLAES values. In one of the three cases (May 29, 1992) it looks as though the CLAES may be registered too low by about a kilometer. These three cases taken together suggest CLAES peak vmr systematically low, on the average, compared to FIRS-2 by about 0.5 ppbv.

A single comparison with the BLISS data is shown for August 26, 1992, in Figure 10. The CLAES profile is within 1° latitude, 2° longitude, and 1 hour of the mean time and position for the BLISS data. CLAES and BLISS agree within the combined instrumental error estimate limits, i.e., approximately 1 ppbv near 30 mbar and 0.3 ppbv near 7 mbar. Again, for this one case, CLAES near peak vmr may be systematically lower than BLISS by about 0.5 ppbv.

Comparison with data from the SLS instrument is shown in Figure 11 for September 29, 1992, and April 3, 1993. The CLAES profiles are within 2° latitude and 6° longitude and 6 hours of the mean times and positions reported for the SLS instrument. The general shape of the two profiles is much the same. Agreement is achieved within better than the reported SLS error estimates (approximately 1 ppbv or less at and above the altitude of the peak mixing ratio and increasing below the peak mixing ratio to almost 2 ppbv) over the entire profile for September 29. The same is true for the April 3, 1993, case except for three points on the top side near 27, 29.5, and 32.2 km altitude that have the look of being registered 2 to 3 km higher than the corresponding CLAES data. Once again, the trend is for CLAES to look systematically low in peak vmr by approximately 0.5 to 1.0 ppbv.

Comparisons of CLAES profiles with data from the MkIV instrument are shown in Figure 12 for September 15, 1992, and April 4, 1993. The CLAES profiles are within 2° latitude, 2° longitude, and 11 hours of the mean times and positions reported for the MkIV instrument. For the September 15, 1992, case the MkIV sunset peak occurs at about the same altitude as the CLAES, the sunrise peak about 1.6 km higher. For the April 4, 1993, case, altitude registration relative to the peak vmr appears within 0.1 km, with CLAES peak vmr at higher altitude this time. Considering all three profiles, the vmr agrees within the relatively small combined estimated instrumental error for most of the points. In these comparisons the average CLAES peak vmr is low by about 0.4 ppbv.

A comparison of CLAES versus two Murcray Bomem FTS profiles obtained July 24, 1992, in a launch from Palestine, Texas (31.6°N, 259.5°E), and April 8, 1993, in a launch from Barstow (Daggett Airport), California (35.4°N, 253.7°E), is shown in Figure 13. The agreement between CLAES and FTS data is generally good except on the bottom side for April 8, 1993.

Comparison with northern winter high-latitude profiles measured by balloon-borne instrumentation: A series of comparisons with profiles obtained by the CAESR instrument near Kiruna, Sweden, is shown in Figure 14. The profiles were obtained on January 9, March 5, March 12, and March 14, 1992. The CLAES profiles shown for comparison are within 2° latitude, 1° to 40° longitude, and 8 hours of the CAESR profiles. The January 9, 1992, comparison is shown in Figure 14a and the two instruments agree within the combined estimated instrumental error for all points above 16 km. This is an example of rather unusual profiles but is not too surprising considering the highly dynamic north winter high-latitude conditions, with potential for further transient perturbation due to denitrification and sedimentation in air passing through very cold regions. For example, high latitude in situ HNO_3 measurements on February 13, 1992, were reported by *Spreng and Arnold* [1994] in which the ascending and descending peak vmr were approximately 7 and 19 ppbv, respectively, and where ascent and descent were separated by about 200 km. In the March 5, 1992, comparison the magnitudes of the peak vmr are very similar even though they occur at altitudes that differ by 2 km. Although the altitudes of the peak vmr are quite different, the altitude of the local minimum near 22 km is the same in each data set, and considering the potential effects on the comparison of small-scale spatial and temporal variability, it is difficult to judge whether there is a significant difference in the registration in the two data sets. Next, in the comparison for March 5, 1992, most of the data agree within the combined estimated instrumental error. Again, there is a relatively large displacement in the altitude of the peak vmr, but the very good top side and bottom side agreement argues that misregistration

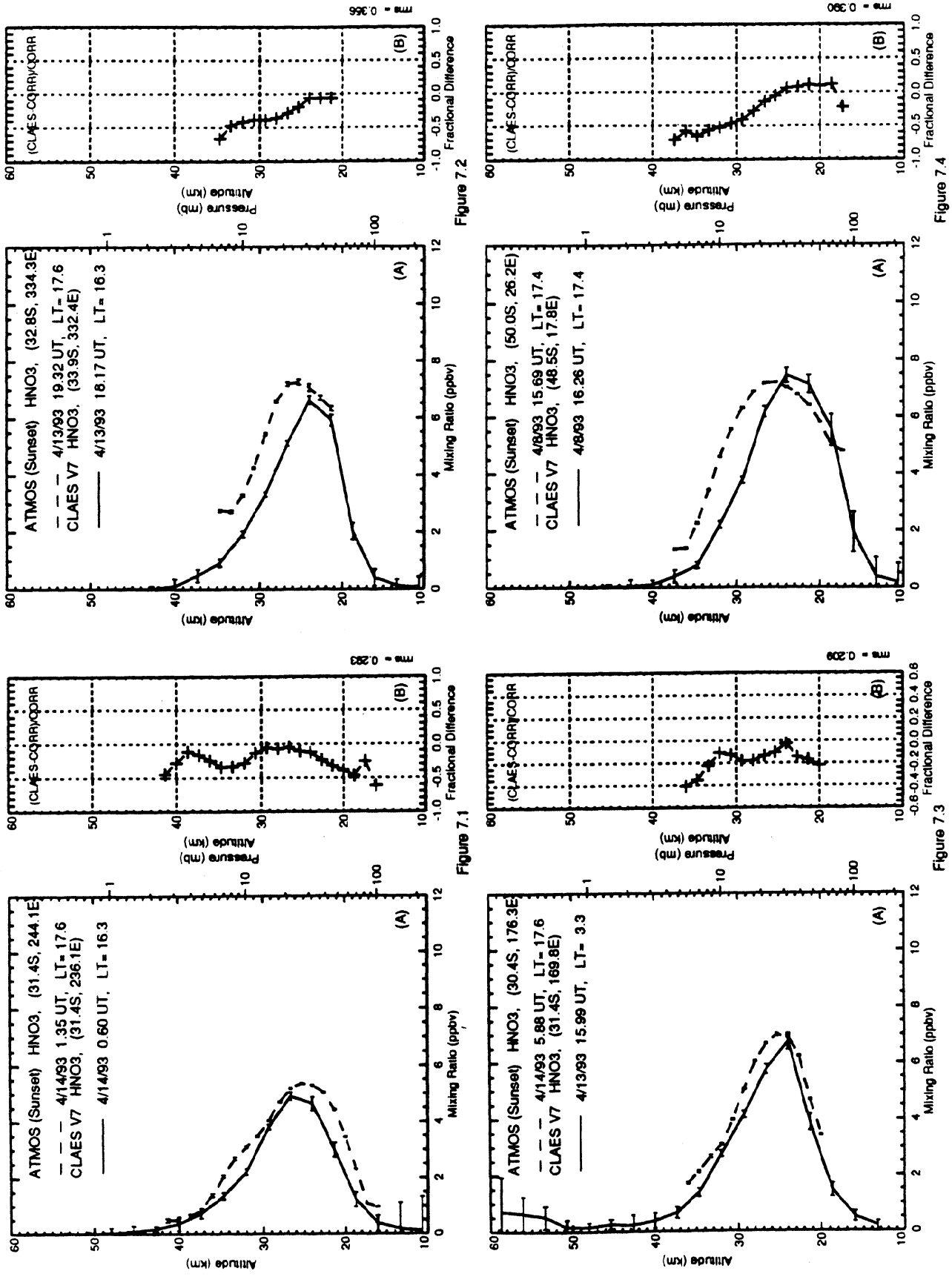

Figure 7.1

Figure 7.2

Figure 7.3

Figure 7.4

Figure 7. Four representative profile comparisons of CLAES to 1993 ATMOS sunset data.

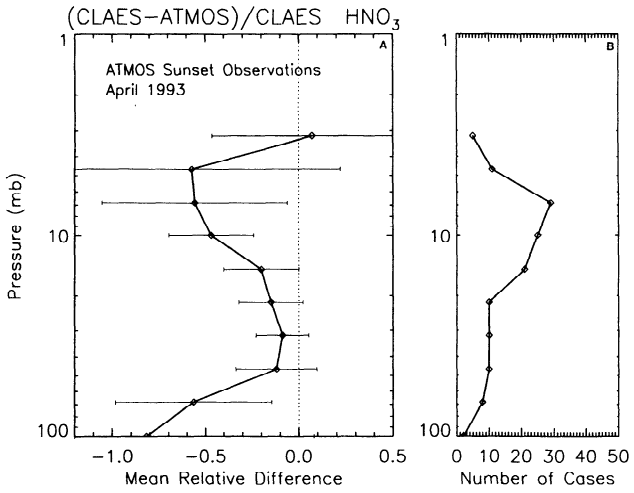

Figure 8. As in Figure 4 but for the 1993 ATMOS sunset data.

is not so much a factor in the peak displacement as is variability. The March 12, 1992, case provides the best comparison of the four and suggests that registration is good within a small fraction of a kilometer and shows agreement with all data points well within combined estimated instrumental error. The March 14, 1992, case also shows very good agreement, not quite so good as the March 12 case. Considering the generally good and sometimes very good top and bottom side agreement in all four cases, registration is in agreement to 1 km or better and within variability. Averaging the four cases, the CLAES peak vmr is 12.0 ± 0.9 ppbv and is larger than the average CAESR peak vmr by 7 ± 10%.

Data from the MIPAS-B instrument for January 12–13 and for March 14–15, 1992, are compared with CLAES profiles in Figure 15. The latter case is shown in Figure 15a. The CLAES profile estimated to be closest to tangent point location of the MIPAS-B measurement and viewing in the same direction was used for the comparison. The agreement is within the combined estimated instrumental error for all but the highest-altitude points. The CLAES may be registered high, but it is difficult to be conclusive due to data sparsity. There were no CLAES data obtained on January 13, but data from January 12, when CLAES data were obtained for only a partial day prior to closing the telescope door in preparation for the space craft yaw around, with selection criteria as for the March comparison, are shown in comparison with the MIPAS-B data in Figure 13b. This is a good comparison considering the 1-day time delay between measurements and that the time period, coincident with the beginning of breakup of a stratospheric warming, was even more disturbed than usual for north high-latitude winter conditions. However, because of the time delay this comparison will be considered less meaningful for quantitative evaluation in the subsequent discussion.

Summary of comparisons with correlative profiles: The results for registration and vmr comparison at 70 mbar, the altitude of peak vmr and 10 mbar are summarized in Table 2. Registration versus the balloon profiles and the ATMOS 92 sunset case is within 0.4 km. The registration offset is larger for the ATMOS 92 sunrise and ATMOS 93 sunset cases, but as mentioned above, very few of these were processed to a low enough altitude to be used for registration purposes. Good peak vmr agreement is achieved in all cases. The CLAES values tend to be less than correlative for cases where the CLAES peak vmr is approximately ≤8 ppbv. In all these cases, namely, ATMOS 92 sunrise, ATMOS 93 sunset, and midlatitude balloons, agreement within variability is just missed. Conversely, for CLAES peak vmr approximately ≥10 ppbv, the tendency is for the CLAES values to be slightly larger than correlative but to agree within variability. At both 70 and 10 mbar the CLAES vmr agrees within variability with the balloon measurements. Agreement within variability is achieved in three of five ATMOS cases. The variabilities are larger than in the case of the balloon comparisons. As shown in Figures 4, 6, and 8, from 10 to 3 mbar, the large majority of the data points from midlatitude balloons agree within the combined instrumental error estimate and the majority of comparisons with ATMOS within variability. There were five midlatitude balloon profiles down to 100 mbar and, on the average, CLAES was less by 24 ± 35%. None of the midlatitude profiles went lower than 119 mbar. At high latitude, three of the four CAESR profiles went down to 100 mbar and there CLAES was less, on the average, by 33 ± 10%. The CLAES profiles obtained for comparison with the MIPAS-B were in such disturbed conditions that retrieval below 70 mbar was not meaningful, which is indicated by the large error bars there, as shown by Figures 15a and 15b.

3.2.2. Comparison with LIMS zonal mean vmr. Although CLAES and LIMS occurred 13 to 14 years apart, there are some useful things to learn by comparing the two data sets on a zonal mean basis. Figure 16 is shown to compare zonal means from four polar winters: CLAES January 10, 1992, in Figure 16a; CLAES January 5, 1993, in Figure 16b; LIMS January 10, 1979, in Figure 16c; and CLAES July 10, 1992, in Figure 16d. First addressing the north winter cases, the general structure of the three zonal means is very similar, with some differences, and with some striking year-to-year differences. The CLAES has more HNO_3 than the LIMS in both cases near the north pole, and particularly so in the 1993 case. Similarly, the CLAES seems registered to generally lower altitude (≈40 mbar) in the high-latitude north than LIMS (≈30 mbar). The LIMS and CLAES 93 show a prominent positive horizontal gradient poleward from about 50°N at altitudes near 10 mbar, and above. There is just a hint of this in the CLAES 92. Finally, at the altitude near peak vmr the CLAES 92 has about 30 to 60% more HNO_3 in the region from the equator to 32°S than the LIMS or CLAES 93. The latter pair look very similar through this region.

The CLAES July 10, 1992, in Figure 16d provides a classic example of south polar winter HNO_3 depletion due to freeze-out on PSCs. There is a large maximum in the so-called collar region near 62°S and at 30 mbar that is unique to the south polar winter. Similar to the CLAES 93 and the LIMS, it shows a prominent positive horizontal gradient poleward from about 50°S at altitudes near 10 mbar and above. In the region from the equator to 32°N it more closely resembles the relatively enhanced CLAES January 10, 1992, equator to 32°S case than the other two north polar winter examples.

Figure 17 is shown to compare zonal means for early southern autumn conditions, just past equinox, for three cases: CLAES April 1, 1992, in Figure 17a; LIMS April 4, 1979, in Figure 17b; and CLAES April 6, 1993, in Figure 17c. Again, the general structure of the three zonal means is very similar. A notable difference for both the January and the April comparisons, however, is that the top side and bottom side vertical gradients are steeper than LIMS. Consistent with discussion

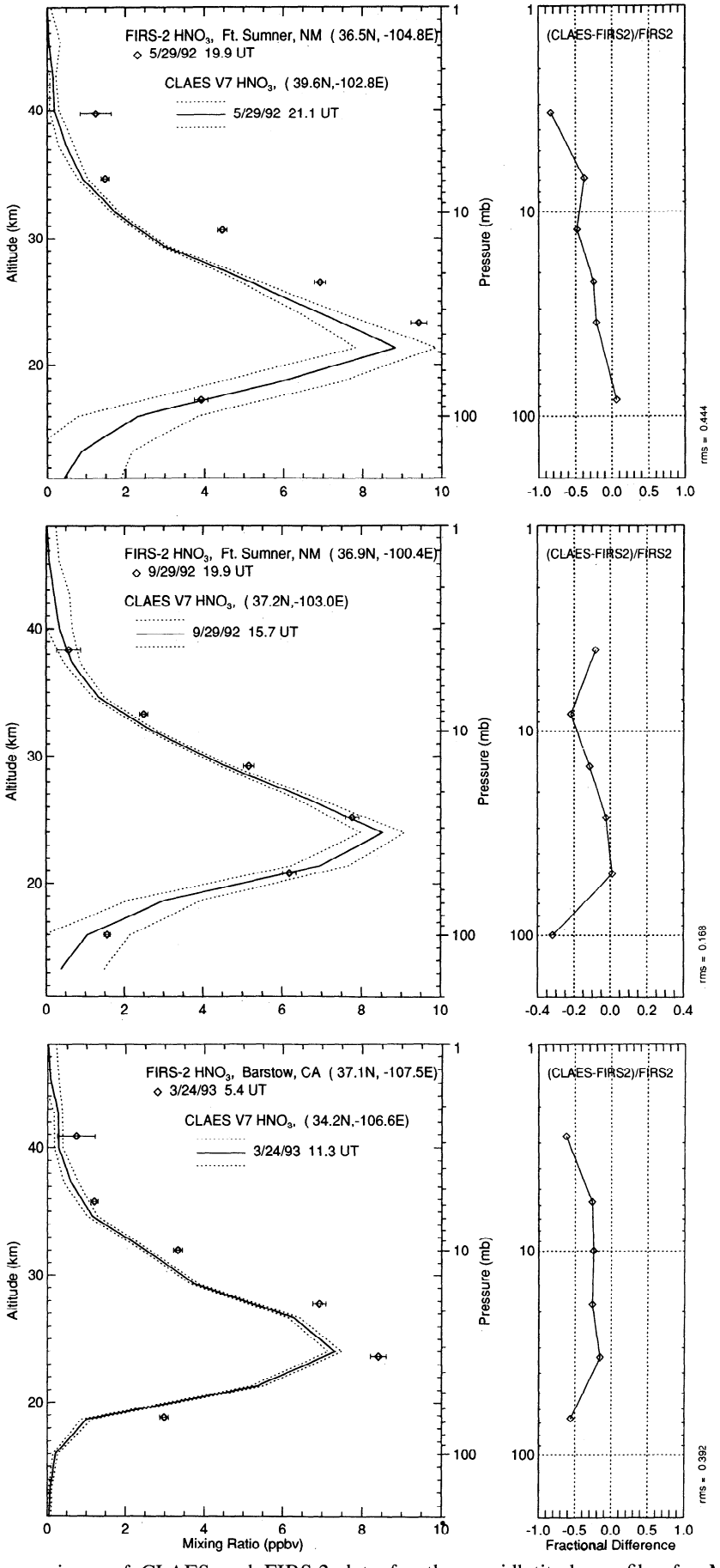

Figure 9. Comparisons of CLAES and FIRS-2 data for three midlatitude profiles for May 29, 1992, September 29, 1992, and March 24, 1993.

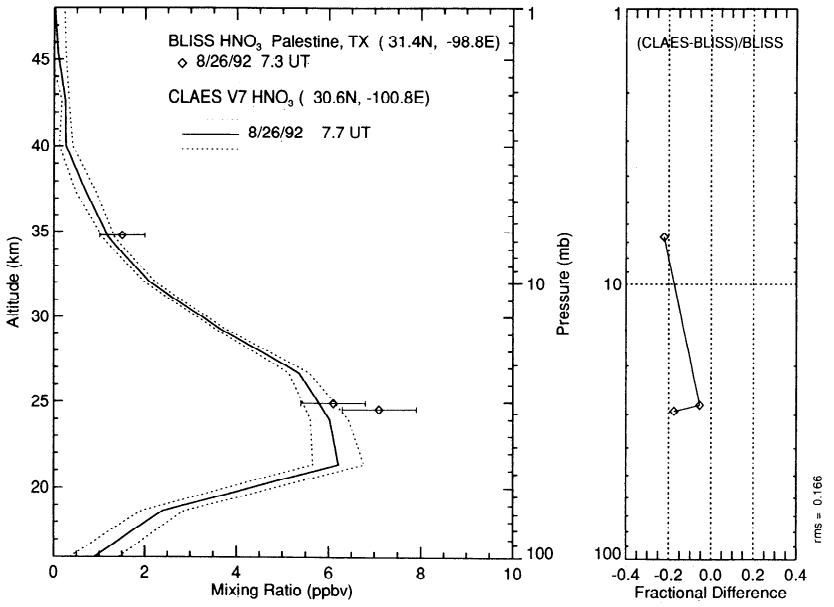

Figure 10. Comparisons of CLAES and BLISS data for a midlatitude case on August 26, 1992.

above, the CLAES 92 has considerably more HNO_3 in the southern hemisphere (≈12 ppbv peak vmr at 64°S as compared to slightly >9 ppbv there for LIMS and slightly <9 ppbv there for CLAES 93, for example). Next, at 32°N the CLAES 92 peak vmr (>6 ppbv) is the largest of the three cases, the LIMS 79 is intermediate (≈6 ppbv) and the CLAES 93 is least (>5 ppbv), but these contrasts are small compared to the southern hemisphere. These April cases are also useful in that they correspond to time periods when ATMOS data were obtained in 1992 and 1993. As discussed above, the April 1992 to 1993 trends noted in the CLAES data were corroborated, by the ATMOS data.

These comparisons show that except for some details, as discussed above, the CLAES and LIMS zonal means are generally similar. It is seen that except for north middle and high latitudes, there is a significant decrease in the HNO_3 observed by CLAES from 1992 to the corresponding time in 1993. In these cases the LIMS much more closely resembles the CLAES 1993 cases. Polar winter enhancements above 10 mbar and from 50° poleward are seen to occur quite prominently in three of four cases and also to a much lesser extent in the north CLAES 92 case.

4. Error Estimation Based on Instrument Characterization

In estimating errors associated with the retrieval of HNO_3 the approach was to take the estimated errors in the measured and calculated atmospheric spectral radiances and apply them to an altitude dependent profile relating percent error in HNO_3 to vmr percent radiance error. This latter relationship is found empirically by determining the sensitivity of the retrieved HNO_3 vmr to changes in the input radiance to the retrieval algorithm. Estimated errors in the vertical location of the detector footprints at the Earth limb are translated into approximate HNO_3 vmr errors using climatological HNO_3 vertical profiles. In the discussion below we first provide estimates for radiance errors, then summarize the resulting errors in retrieved HNO_3 vmr in Table 3.

4.1. Systematic Errors

The primary sources of systematic error are as follows:

4.1.1. Radiometric calibration. This has been discussed in numerous references [*Roche et al.*, 1993a], including a discussion [*Sterritt et al.*, 1990] of the design and prelaunch characterization of the onboard blackbody calibration source (OBCS), and a paper discussing the details is in preparation. Briefly, the OBCS is an aperture size blackbody calibrator that is mounted on the inside of the CLAES door. When the door is closed, the OBCS fills the instrument FOV, and CLAES is operated in the radiometric calibration mode. In this mode, blackbody calibrator data are taken on every other 65 s UARS repeat cycle in an operation that is identical with that of the CLAES nominal science mode. CLAES radiometric calibration parameters are obtained by a least squares fit of count rate to blackbody radiance as the door-mounted OBCS cools to equilibrium each time the door is shut. About 24 hours is required to cool to equilibrium. The calibration data obtained in this way for the 50 spectral channels utilized by the CLAES science mode for the 20 detectors are used to derive calibration parameters for each combination of detector and spectral channel. In operation the calibration data were obtained when the instrument telescope aperture door was closed for each spacecraft yaw and also when it was closed for 1 to 2 days halfway between the yaws for the purpose of calibration.

When the door is open, the calibrator equilibrates at 245 K, and when the door is closed, the calibrator cools down to equilibration of the order of 150 to 160 K, depending on the solar beta angle. However, early in the mission when the cryogen was colder than its equilibrium temperature, this number was more like 145 K. The Earth-limb radiance at the higher altitudes for some of the longer-wavelength channels is less than radiated by the blackbody even at its coldest temperatures. In this case, the quantitative behavior of the detectors at low-radiance levels encountered at the shorter wavelengths was used to construct a detector characteristic curve that could be used to extrapolate to optimal calibration for the long wave channels for the low-radiance case.

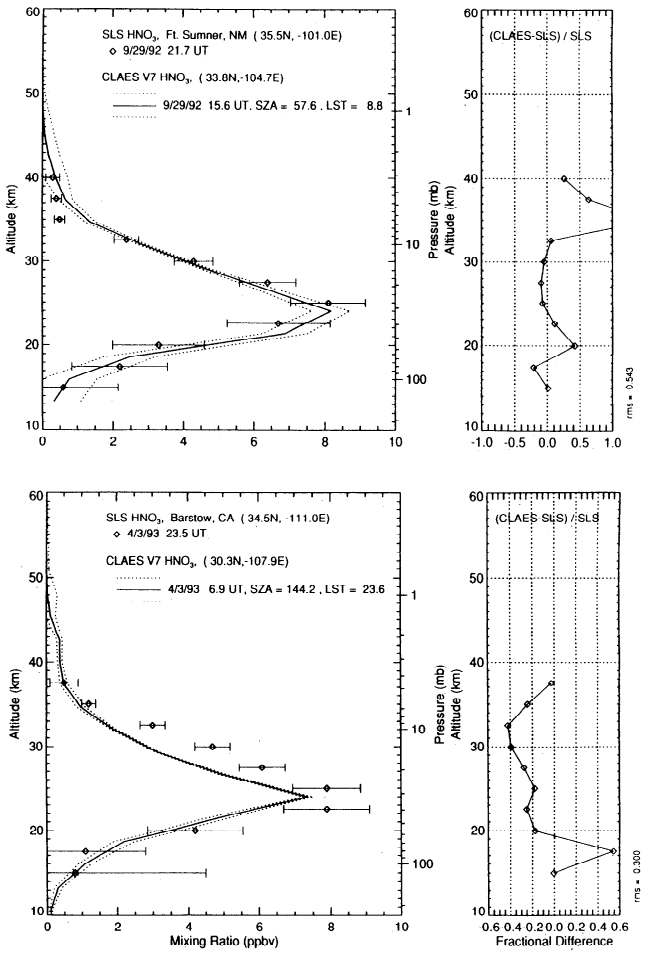

Figure 11. Comparisons of CLAES and SLS data for two midlatitude cases on September 29, 1992, and April 3, 1993.

Uncertainty in the determination of spectral radiances from this source involves (1) biases in the OBCS temperature as determined from five platinum resistance thermometers (PRTs), (2) errors in the knowledge of the absolute emissivity, (3) offsets in the electronic zero-photon level, (4) uncertainty in foreoptics thermal emission, and (5) the use of a detector "characteristic responsivity curve" fitting technique to provide responsivities for atmospheric radiances below the minimum (coldest) OBCS radiance. As discussed by *Sterritt et al.* [1990], temperature and emissivity uncertainties in the 879 cm^{-1} HNO_3 spectral channel amount to approximately 1% RSS radiance error at the OBCS coldest temperatures. Offsets in the electronic zero-photon level and uncertainty in foreoptics thermal emission combine for 2×10^{-9} W cm^{-2} sr^{-1} cm^{-1}. The other uncertainties listed above are mainly of interest in this wavelength region for higher-altitude low-radiance conditions where there is little or no sensible HNO_3. The RSS of all radiometric calibration radiance errors is estimated to be of the order of 1, 1, 1.7, and 28% at 70, 30, 10, and 3 mbar, respectively.

4.1.2. Uncompensated drift in radiometric calibration. As noted previously, radiometric calibrations were performed approximately every 2 weeks throughout the lifetime of the mission. Inspection of these data typically shows less than 1% system responsivity change from calibration to calibration, although over periods of many months the responsivity can drift by as much as 7% in a particular direction. For the V7 software that was used in the retrieval of the data discussed here, this drift was compensated for all days prior to August 10, 1992. All data obtained beyond this point, however, were calibrated using the August 10 parameters, uncompensated for drift. In the next version of the retrieval software the calibrations through the remainder of the mission will be incorporated, thereby providing drift compensation for data obtained beyond August 10, 1992. However, in the V7 data this artificial contribution to apparent trend is present. For the CLAES instrument HNO_3 retrieval channels near 879 cm^{-1} the uncompensated drift is small in the period from August 10, 1992, to January 7, 1993, with system responsivity decreasing approximately linearly over that period by 0.6%. In the period from January 7 to April 4, 1993, the system responsivity continues to decrease, approximately linearly, from 0.6% to a maximum of 3.7%. This is followed by recovery to the August 10, 1992, value by April 24, 1993. The vmr is biased low by a maximum that corresponds to the maximum decreased uncompensated responsivity of 3.7% by approximately 6.3, 5.2, 3.7, and 3.7% at 70, 30, 10, and 3 mbar.

4.1.3. Instrument characterization. This includes (1) absolute wavelength calibration, (2) spectral transmission function, (3) spectral dispersion along the array vertical extent, (4) detector spatial responsivity, (5) optics out of field stray light rejection, and (6) in-field scattering (optical cross talk). *James et al.* [1988] discuss the design and prelaunch characterization of the CLAES solid Fabry-Perot etalons, and *Mergenthaler et al.* [1990] and *Kumer et al.* [1990] discuss aspects of the design and prelaunch characterization of the blocking filters. Information on the absolute wavelength calibration and the effective spectral transmission function can also be deduced from on-orbit spectral scans of specific emission features, and limits on off-axis and in-field scattering can be deduced on orbit from high-altitude and "cold space" radiance measurements.

1. From prelaunch and on-orbit analysis we estimate an uncertainty of 0.01 cm^{-1} in the absolute spectral calibration which results in a relatively small radiance error of <0.6%.

2. Similarly, we estimate an uncertainty of 0.0075 cm^{-1} in the spectral function width which represents a 3% error in the nominal 0.25 cm^{-1} etalon function full width at half maximum. The error has some covariance between the measurement of atmospheric spectra and the measurement of the near-continuumlike radiance from the OCBS especially for quasi-continuum atmospheric emitters such as aerosol and CFCl3, and in the wings of overlapping lines. This would tend to reduce the effective radiance error associated with the spectral function uncertainty in these situations. However, for the purposes of comparing estimated systematic error with that inferred from correlative measurements we will assume the maximum error of 3% for the purpose of this estimation.

3. Array dispersion effects contribute less than 1% radiance error.

4. Detector uniformity contributes from 3% at the lowest surface to 0.5% at higher altitudes.

5. Array cross talk contributes less than 0.2% at lower altitudes, increasing to 0.4% near 10 mbar and approaching 1% near 3 mbar.

The RSS of all instrument characterization radiance uncertainties is estimated to be in the range 4.5 to 3.3% between 100 and 0.46 mbar.

4.1.4. Spectral parameters. The parameters used in the CLAES V7 HNO_3 retrieval are a hybrid of the HITRAN92 lines [*Goldman and Rinsland*, 1992] and recent improvements

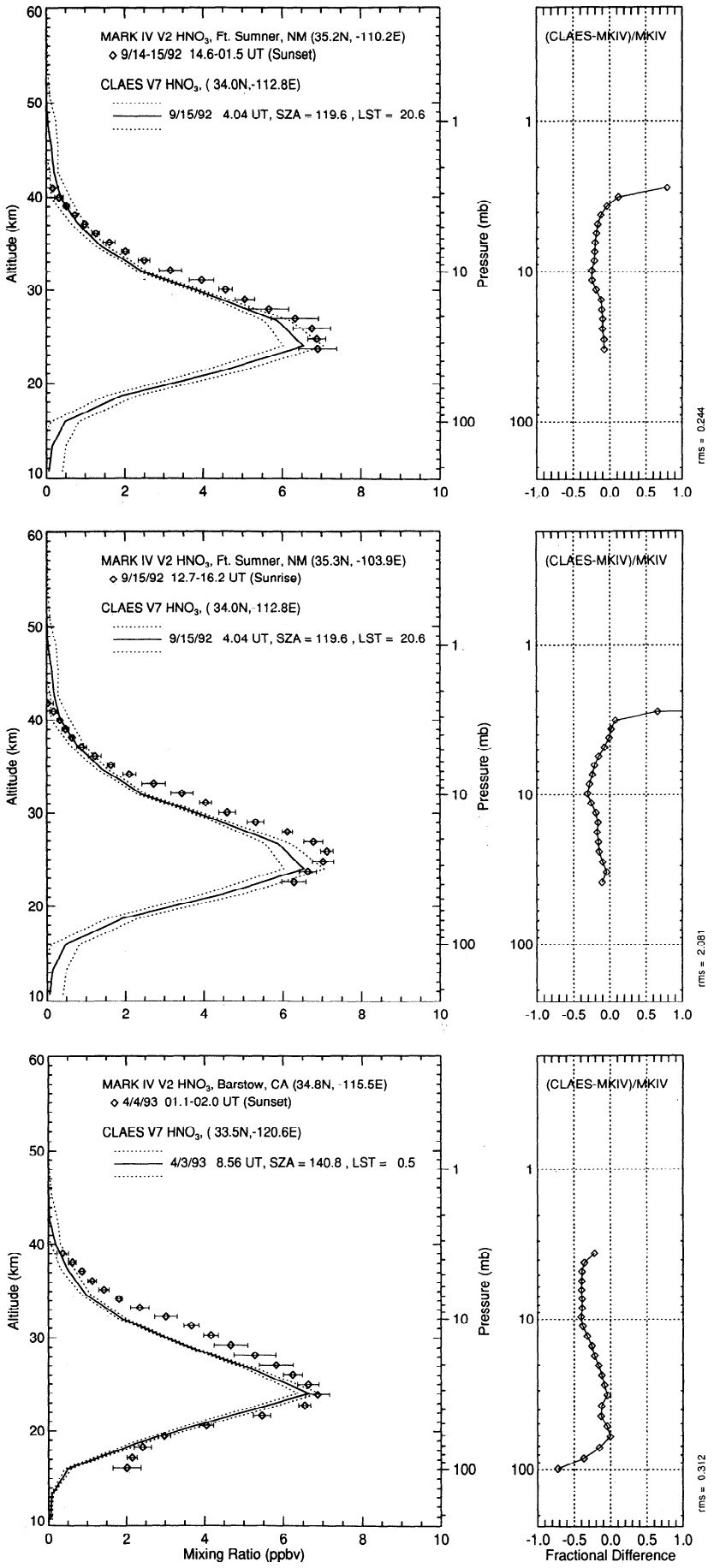

Figure 12. Comparisons of CLAES and MkIV data for three midlatitude cases on sunset and sunrise of September 15, 1992, and on sunset of April 4, 1993.

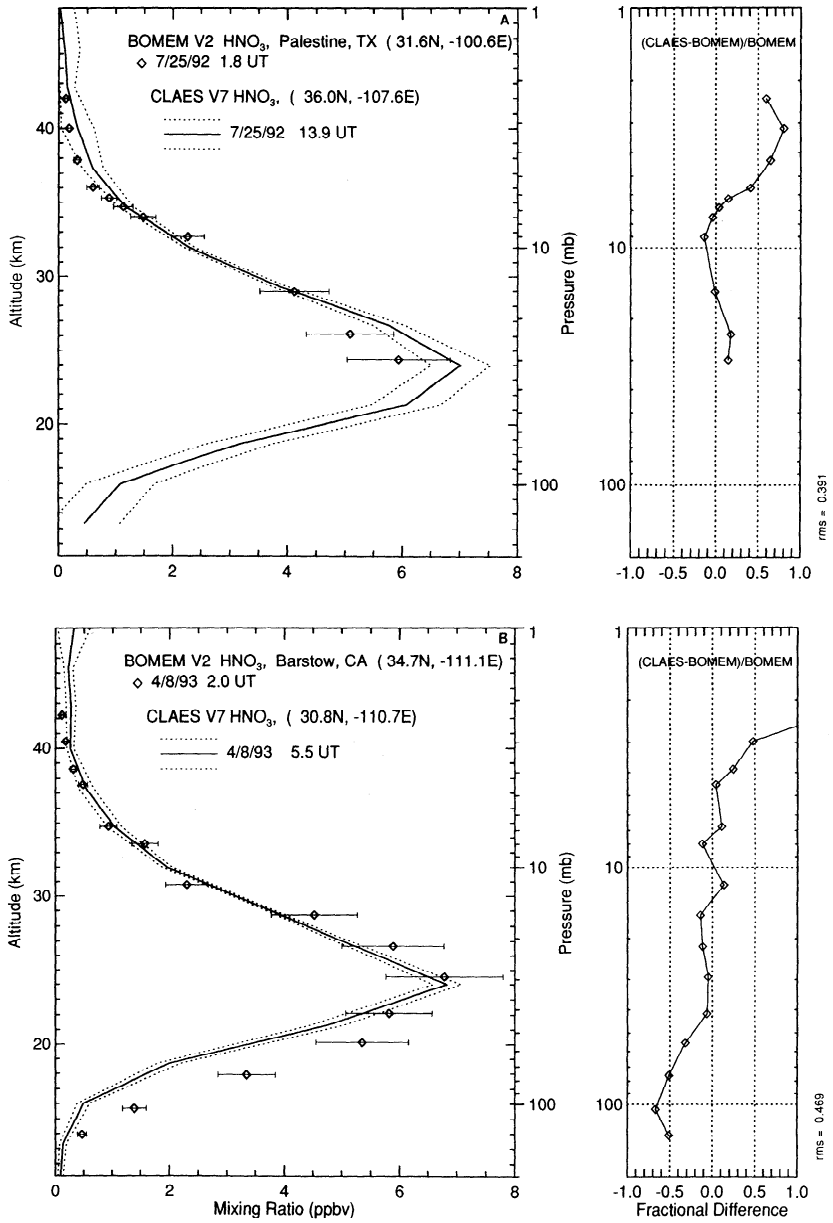

Figure 13. Comparisons of CLAES and D. U. Bomem FTIR data for two midlatitude cases on (a) July 24, 1992, and (b) April 8, 1993.

[*Goldman et al.*, 1994]. By use of these most recent lines [*Goldman et al.*, 1994] achieved better agreement with atmospheric data than had been achieved previously with the HITRAN92 lines, including improvement in the q branch, the dominant HNO_3 CLAES channel. EGA coefficients had been produced for the CLAES HNO_3 region initially by using the HITRAN92 lines. These were available prior to going into V7 production but did not incorporate the new spectral parameters, or address the exact CLAES sampling spectral positions. For the purpose of V7 these were improved in spectral signature by using a set of scaling factors relative to the q branch that were derived from FASCODE limb radiance calculations using old and new lines and corrected for the sampling positions. The q-branch EGA coefficients were unchanged. The combined band strength of the OLD parameters, used for V7, for the ν_5 and $2\nu_9$ lines, including hot bands, was 2.57×10^{-17} cm^{-1} atm^{-1}. The most recent lines [*Goldman et al.*, 1994] have been scaled to the [*Giver et al.*, 1984] band strength of $(2.59 \pm 0.13) \times 10^{-17}$ cm^{-1} atm^{-1} and divided by 1.30 to correct for the omission of hot bands in the new data. The CLAES q-branch channel dominates the CLAES HNO_3 retrieval. In it the absolute value of the sum of the old line strengths is about 10% greater than the sum of the new line strengths due to the modified overall spectral signature of the new lines. Comparison of q-branch channel curves of growth for the old and new parameters suggests that V7 values are biased too low by about 10% in optically thin regions and by as much as 25% in the optically thickest regions. How this bias may impact correlative comparison with the CLAES HNO_3 V7 data product is discussed below. Apart from the bias, there is also about 5% uncertainty in absolute band strength, as discussed above.

4.1.5. Atmospheric temperature determination. Any systematic error in the retrieval of atmospheric temperature will appear in the forward radiance model as an error in the cal-

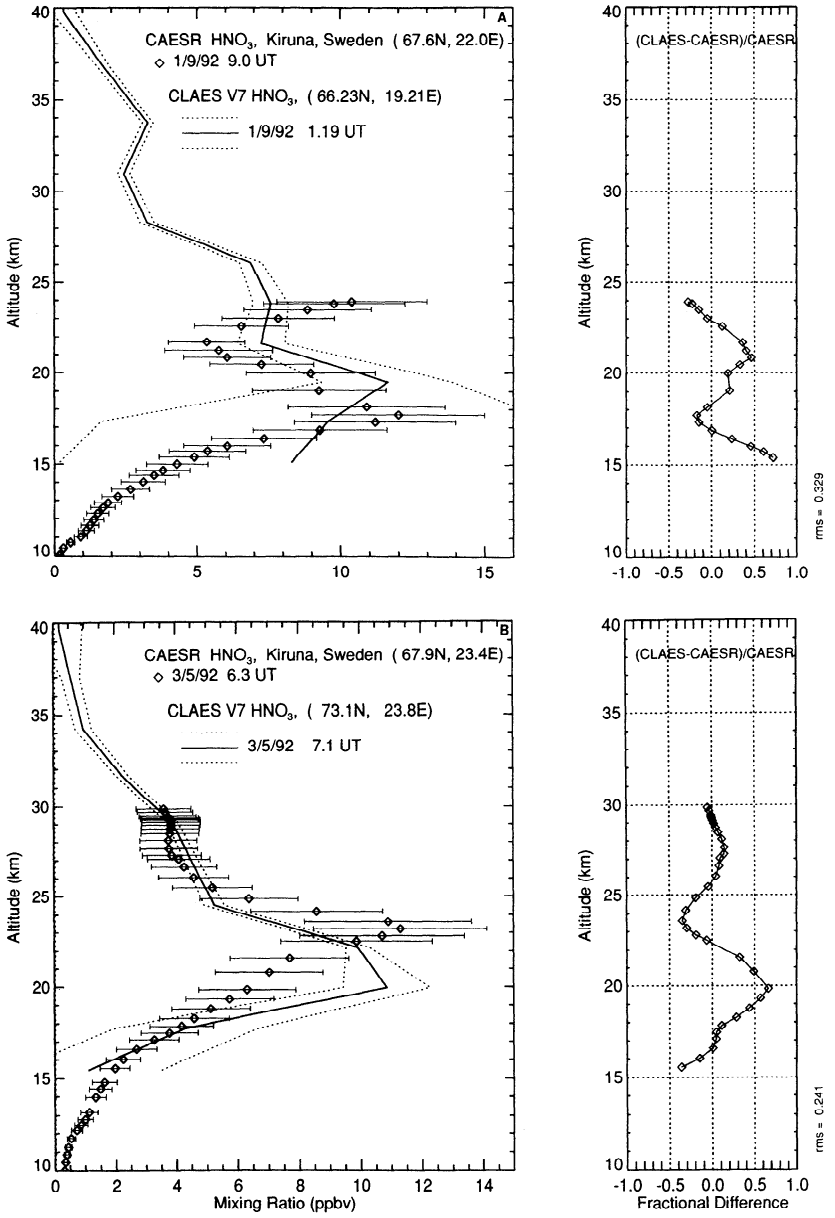

Figure 14. Comparisons of CLAES and CAESR data for four high-latitude northern winter cases on (a) January 9, 1992; (b) March 5, 1992; (c) March 12, 1992; and (d) March 14, 1992.

culation of the HNO_3 radiance. The sensitivity of the radiance error to temperature uncertainty depends on the mean atmospheric temperature at the measurement altitude. CLAES-retrieved systematic temperature errors vary from about 1.9 to 2.3 K in the 100- to 0.46-mbar range [*Gille et al.*, this issue] which results in HNO_3 radiance errors of the order of 3 to 4% for a relatively warm atmosphere of ≈290 K and radiance errors of the order of 8 to 9% for a relatively cool atmosphere of ≈190 K.

4.1.6. Forward radiance model. This primarily involves radiative transfer approximations, treatment of line overlap and mixing, and calculation of EGA table coefficients. Errors are estimated by comparing the forward model results with rigorous line-by-line code calculations, and the order of a 1% systematic radiance error is found.

Table 3 below provides percent systematic error estimates in retrieved HNO_3 volume mixing ratios from these various effects for four pressure levels. The two known biases discussed above are not included in Table 3. These are that (1) the older HNO_3 HITRAN92 lines were used in producing V7 and (2) the uncompensated drift in radiometric calibration commencing August 10, 1992.

As seen from Table 3, the estimated systematic errors in HNO_3-retrieved mixing ratio are dominated by uncertainties in spectral parameters, retrieved temperatures, and spectral response function, with small contributions from the other sources. It is interesting to compare these estimates with the biases identified in the correlative data comparisons, as summarized in Table 2. The estimates are consistent within at least a factor of 2 with the observed biases near the peak vmr. At 70 mbar the estimates and observed biases for the balloon profile comparisons are consistent. At 10 mbar only the CAESR biases, limited to two profiles, are consistent with the estimates. As pointed out in the text above, the differences between V7 and the correlative data have, for the most part, been within the combined error estimates of the instruments, or the vari-

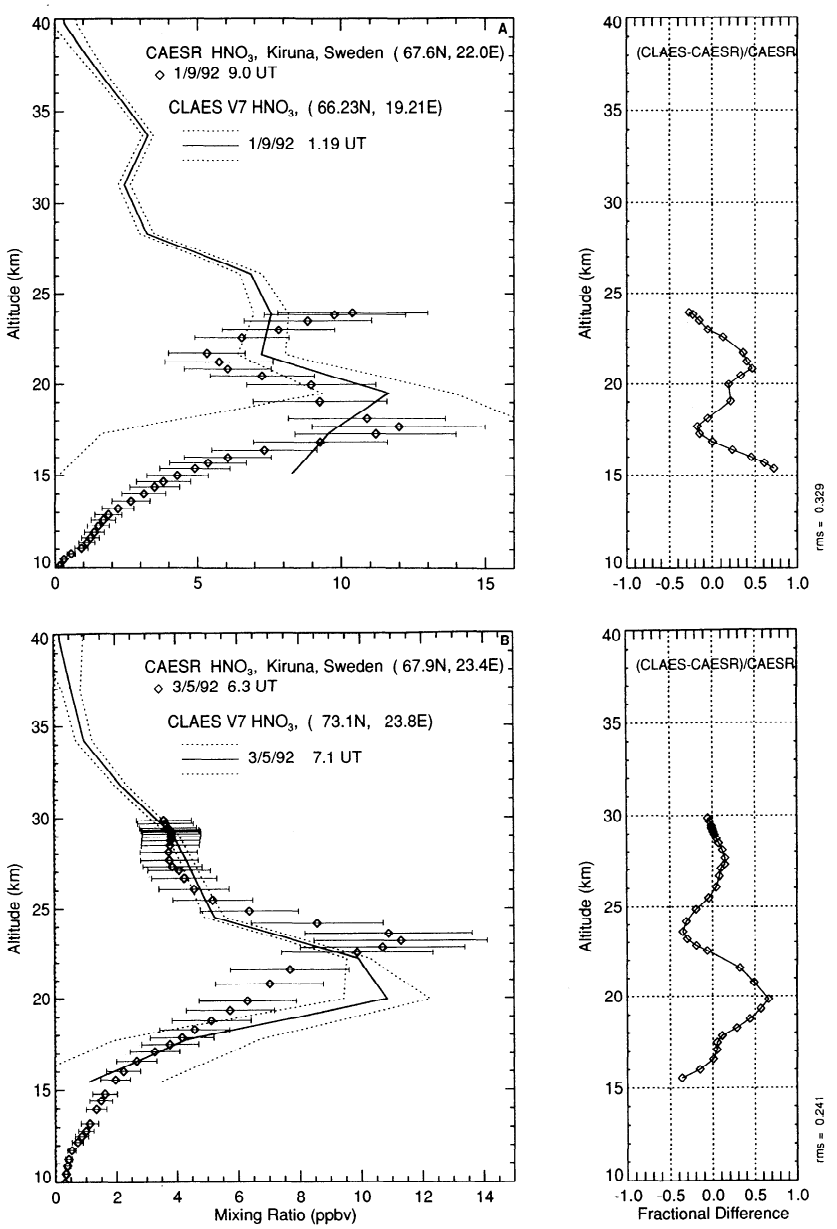

Figure 14. (continued)

ability of multiple measurements. Correcting for the bias low due to V7 spectral parameters would generally improve the agreement for cases of peak vmr approximately ≤8 ppbv in which the CLAES V7 values are generally smaller than the correlative values. However, in the cases where peak vmr are of the order ≥10 ppbv the CLAES V7 are usually about the same or slightly larger than the correlative data, and the spectral parameter correction toward larger CLAES values would not be expected to improve the agreement. This is an issue that will receive careful attention in the development of future and improved software for HNO_3 retrieval.

4.2. Random Errors

4.2.1. Data-derived and algorithmic precision estimates. A repeatability, or precision estimate, may be derived from the retrieved data, independently of the precision estimates that are generated by the preliminary algorithm that is in place in the V7 production software (SW). The technique is described by *Rodgers et al.* [this issue] and exploits the close (≈100 min) time coincidence of the crossing of the ascending and descending limb-viewing track intersects near the midlatitude turnaround. The technique produces a quantity that is probably better interpreted as repeatability. It is pessimistic compared to actual instrument repeatability since it includes atmospheric variability in addition to instrument effects. The upper limit on instrument precision is related to the root-mean-square (RMS) of the differences of the retrieved quantities at this crossing point averaged over a number of days. The periods used for this study included January 9–11, April 15–20, August 8–11 and 25–30, 1992, and January 3–5, and April 1–3, 1993.

The results are shown in Figure 18. For comparison purposes the embedded V7 SW error estimates averaged around the zone at 32°N, or 32°S as appropriate, are shown in Figure 19. It is seen that the precisions as derived from the turnaround data and the production SW error estimates are roughly comparable. The former are typically somewhat the larger of the two below approximately 10 mbar, but the latter can be considerably larger above 10 mbar. Based on the larger values

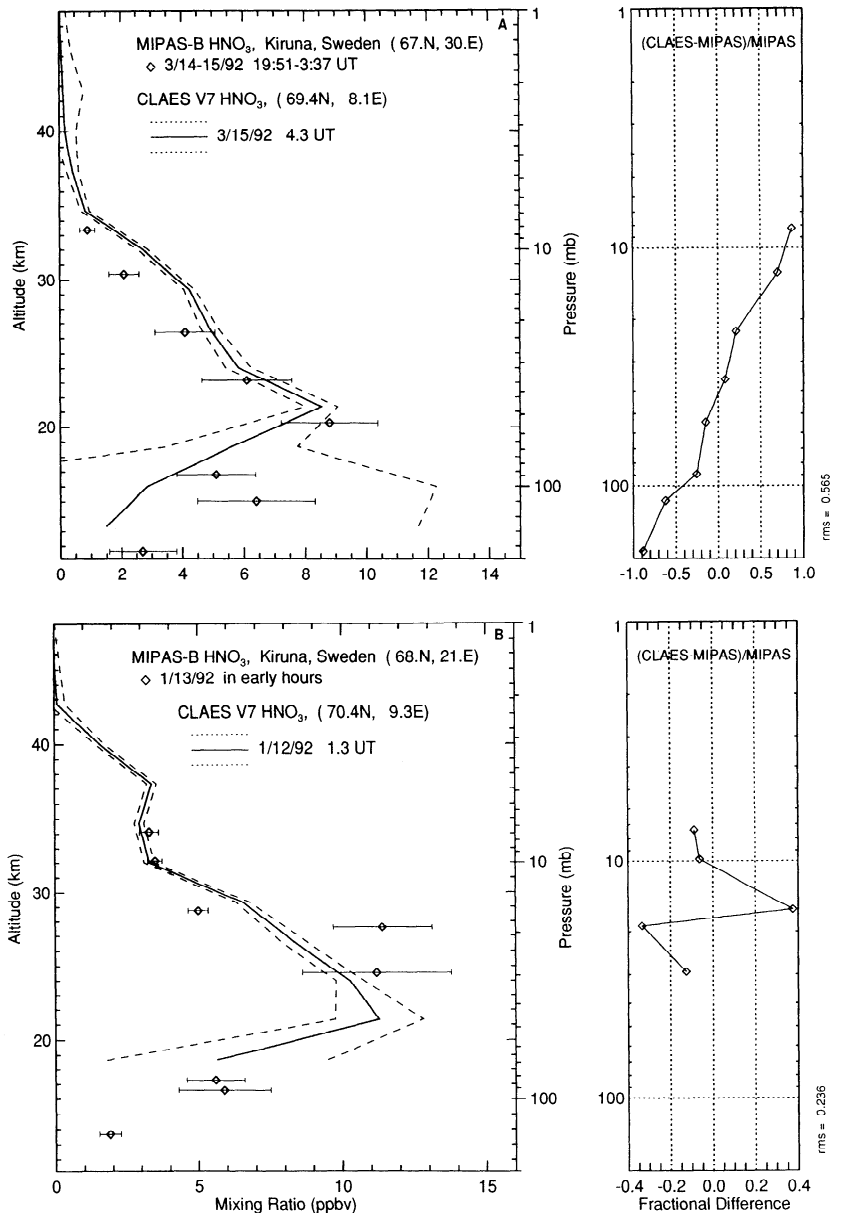

Figure 15. Comparisons of CLAES and MIPAS-B data for two high-latitude northern winter cases on (a) January 12–13, 1992; and (b) March 14–15, 1992.

from the embedded errors near 3 mbar, and the larger values from the turnaround analysis near 70 mbar, we estimate precision on the range from 70 to 3 mbar to be of the order of 0.3 to 1.0 ppbv. In the altitude range above 2 to 5 mbar both types of error estimates approach or exceed 100%.

4.2.2. Random error estimates based on instrument and retrieval characterization. The primary sources of random error are as follows:

Radiometric calibration: The main contributors to random error in the onboard calibration process involve the repeatability of the PRTs that are used for measuring instrument component temperatures and associated electronics and a long-term drift in the OBCS emissivity. For the HNO_3 case, these uncertainties amount to approximately 1.1% RSS radiance error at the OBCS coldest temperature.

Instrument effects: The primary instrument contributors to random errors in the measured radiances involve repeatability in the angular (i.e., spectral) positioning of the Fabry-Perot etalons and detector/signal processing electronics noise. Prelaunch measurements of the angular repeatability showed it to be better than 0.03°, and a similar value was inferred from observations of scatter in the shape of the on-orbit spectral modulation curves obtained during OBCS calibrations. For the HNO_3 spectral channels this results in a random error of less than 1% in radiance. Instrument radiance noise is characterized as the noise equivalent spectral radiance (NESR) in units of W cm^{-2} sr^{-1} cm^{-1}. This is defined as the input spectral radiance at the instrument aperture required to give an output (counts, volts) equal to the system noise for a specific integration time (τ_i). The NESR has a specific value for each of the 20 CLAES detectors and 50 narrowband spectral channels, including the four channels shown in Table 1 above for HNO_3 retrieval. The best measure of the effective NESR is obtained by looking at the variance of a large number of science mode ("mode 1") spectral profiles obtained when the instrument was rolled up to look high above the atmosphere into the cold

Table 2. Summary of Profile Comparisons With Various Correlative Data Sources

Correlative Source	N_{cp}	Note	$Z_{reg} \pm \delta Z$	ACPV	BIAS ± VBIAS Unless Otherwise Noted		
					70 mbar	Peak vmr	10 mbar
ATMOS 92 sunset	17	a	−0.4 ± 1.1	10.25	−55 ± 60	7 ± 11	−40 ± 40
ATMOS 92 sunrise	21	b	−0.7 ± 1.8	4.2		−15 ± 12	−30 ± 20
ATMOS 93 sunset	14		−0.8 ± 1.3	5.4	−60 ± 40	−7 ± 5	−45 ± 20
Midlatitude balloons	11	c	−0.4 ± 0.7	7.5	−17 ± 23	−6 ± 4	−25 ± 14
CAESR	4	d	0.0 ± 1.0	12.0	0 ± 16	7 ± 10	7.5 ± 7.5
MIPAS-B	2	e, f		9.95	−20 and −20	−1 and −5	80 and −10

N_{cp} is the number of profiles available from a given source of correlative data. The averaged offset in registration Z_{reg} in kilometers is negative for CLAES registered lower that the correlative profiles, and its 1σ measurement variability is δZ. ACPV is the average value of the CLAES peak vmr in parts per billion by volume averaged over N_{cp} comparisons. BIAS is the percent difference of the CLAES vmr less the correlative vmr averaged for N_{cp} comparisons. VBIAS is the measurement variability in BIAS. Note a, ATMOS results for 70 and 10 mbar were taken from Figures 4, 6, and 8; note b, data were too sparse for comparison with ATMOS 92 sunrise at 70 mbar; note c, just 6 of 11 midlatitude balloon profiles extended down to 70 mbar; note d, 2 of 4 CAESR profiles extended up to 10 mbar; note e, MIPAS-B data point density versus altitude are too sparse to support statistics on Z_{reg}; note f, percent difference (CLAES vmr − MIPAS-B vmr) for January and March cases are presented for all three pressures.

space region of very low radiances. Using the mode 1 radiance ensures that the identical spectral positions, dwell times, and integration times are obtained as those used when viewing the atmosphere and obtaining the science measurements. Further, these roll-up radiances are conditioned in an identical manner to those used in the retrieval of atmospheric parameters, particularly with respect to the reduction of a quasi-sinusoidal low-frequency artifact ("ripple") seen in the electronics dark noise output. For the 20 detectors times four spectral positions used in the retrieval of HNO_3 in the 879 cm^{-1} channel the array average NESR as seen in the roll-up data lies in the range from 2.3 to 16.4 × 10^{-10} W cm^{-2} sr^{-1} cm^{-1}. We will use the slightly pessimistic value 10 × 10^{-10} W cm^{-2} sr^{-1} cm^{-1} to facilitate the random error estimation discussion.

Vertical smear: During observations a combination of random error in the positioning of LAAM and spacecraft jitter due to array thermal snap results in a vertical jitter of approximately 92 m. The resulting error in mixing ratio will be dependent on the vmr vertical gradient of the species whose line radiances are being observed. For the CLAES HNO_3 we will use the pessimistic scale height value of 6 km which gives the random vmr error of the order of 2%. Note that near the altitude of peak vmr the radiance error will be much less than this.

Horizontal gradients: Random errors due to line of sight gradients in the viewed radiances were investigated by looking at the sensitivity of the retrieval algorithm to induced gradients, leading to an estimate of the order of 1% equivalent

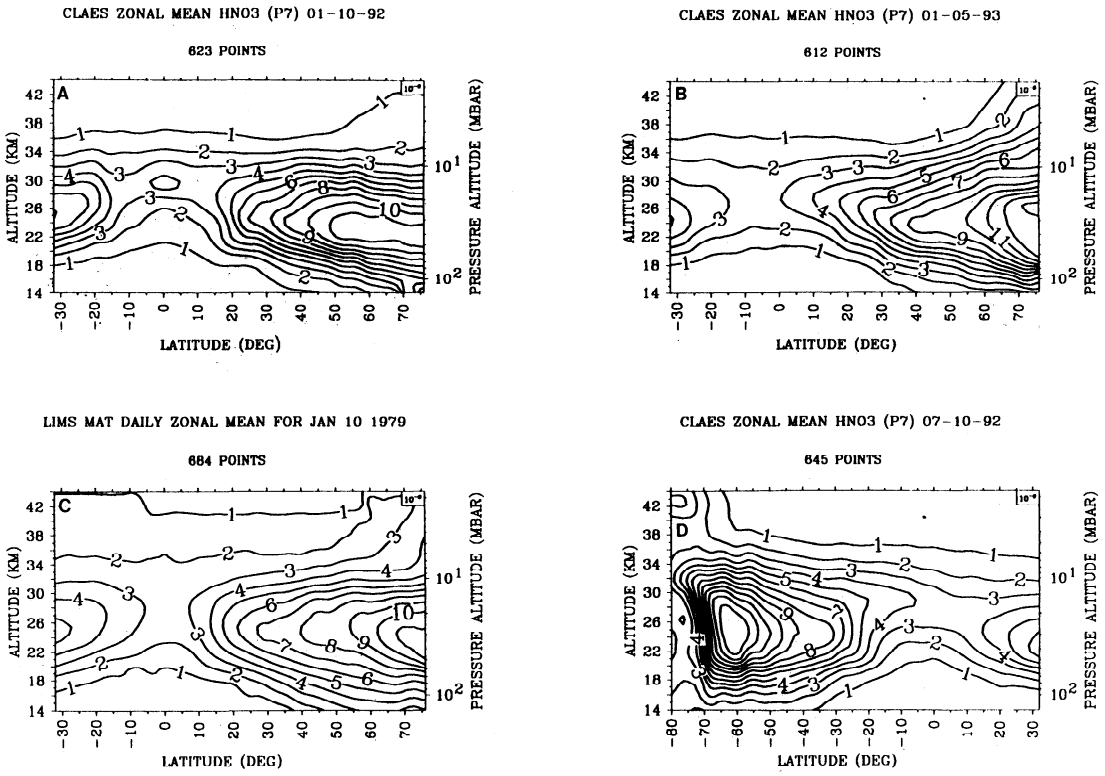

Figure 16. Comparisons of CLAES and LIMS zonal mean cross section data: (a) CLAES on January 10, 1992; (b) CLAES on January 5, 1993; (c) LIMS on January 10, 1979; and (d) CLAES on July 10, 1992.

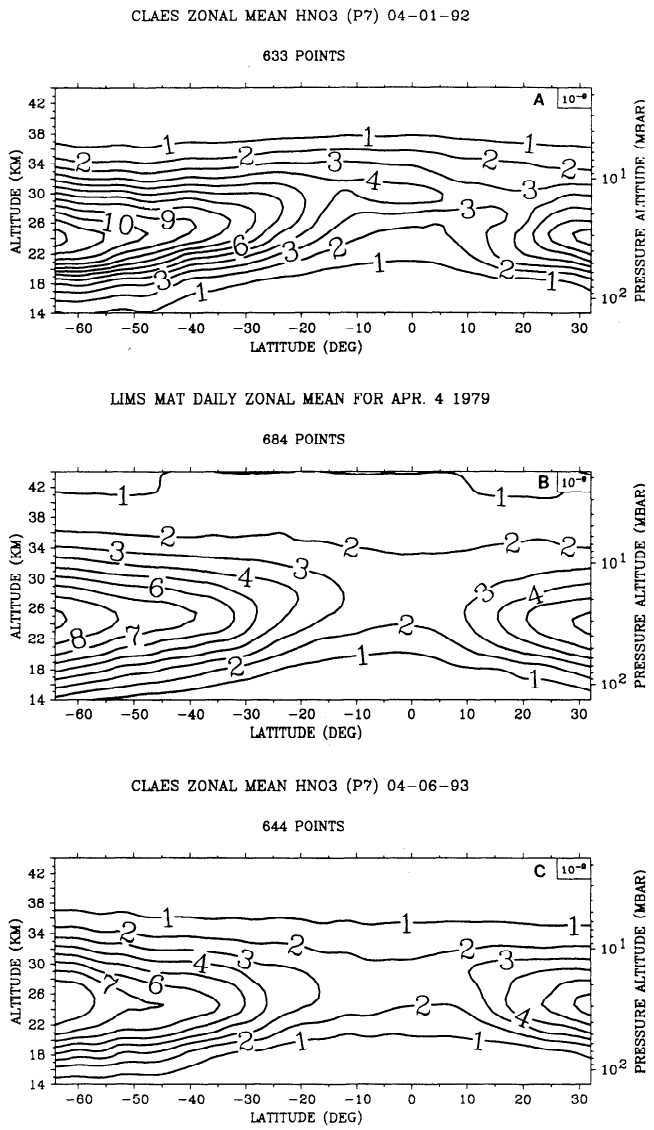

Figure 17. Comparisons of CLAES and LIMS zonal mean cross section data: (a) CLAES on April 1, 1992; (b) LIMS on April 4, 1979; and (c) CLAES on April 6, 1993.

radiance error in relatively benign conditions as encountered in low midlatitudes and in the tropics. The number can be as large as 10% however for extreme conditions such as viewing parallel as compared to viewing perpendicular to PV contours on the edge of the vortex. The benign number applies for most data and is the one used for the overall estimates, as summarized below in Table 4.

Atmospheric temperature determination: CLAES-retrieved random temperature errors vary from about 0.6 to 0.8 K in the 100- to 0.46-mbar range [*Gille et al.*, this issue] which results in HNO_3 radiance errors of the order of 2%. Table 4 provides percent random error estimates in retrieved HNO_3 volume mixing ratios from these various effects for four pressure levels.

It is interesting to compare the estimated random error, or precision in the CLAES HNO_3 retrieval as shown in Table 4 with the repeatability as shown in Figure 18 that is derived from observed variances in the retrieved HNO_3 at the subtropic 32°N and 32°S latitude turnaround points. For the six cases shown in Figure 18 the estimate at 70 mbar is optimistic by about a factor of 2. At 30 and 10 mbar the estimate is about the same as the turnaround numbers, or slightly pessimistic. At 3 mbar the estimate is similar to what is seen in four of the six cases, and optimistic by about a factor of 2 for the two cases, August 8–11, 1992, and April 1–3, 1993.

5. Data Usage, 1992–1993 Trend Discussion and Usage Caveats

5.1. Trend Discussion

Trends in data sets may indicate important physical and chemical atmospheric processes and therefore when these are noted in the data set, as is the case for CLAES HNO_3, there should be comparisons with available correlative data, and some study of candidate trend mechanisms, to verify that the observed trends and their characteristics, are reasonable.

5.1.1. 1992 to 1993 trends in the profile comparisons. In the comparisons with the ATMOS 92 and 93 sunset data that were obtained in consecutive years at almost the same time of year and place, as discussed in section 3.2.1, similar trends were noted in both the CLAES and the ATMOS data. Near 50°S, several profiles were obtained nearly coincident with ATMOS in the April time frame in 1992 and 1993, and these gave a trend ratio of peak vmr from 1992 to 1993 in the CLAES data of 1.48 (i.e., a 48% decrease in peak vmr from 1992 to 1993) and in the ATMOS data of 1.34. Similarly, near 31°S the CLAES and ATMOS 1992 to 1993 trend ratios were 1.35 and 1.44, respectively. As discussed above, the CLAES April 1993 peak vmr must be adjusted upward by about 5% to account for the uncompensated drift in radiometric calibration. This reduces the apparent CLAES trend ratios at 50°S and 31°S to 1.41 and 1.28, respectively. These agree well with the ATMOS trend ratios in the sense of the trend, decrease from 1992 to 1993, and quantitatively within the data variability.

As discussed in section 3.2.1, among the comparisons with correlative data obtained by balloon-borne sensors, only the FIRS-2 provided cases nearly a year apart on May 29, 1992, and March 24, 1993. Seasonal behavior would predict an increase in peak vmr from May 29, 1992, to March 24, 1993, but an actual decreasing trend ratio of peak vmr from 1992 to 1993 of 1.13 and 1.18 were noted in the FIRS-2 and CLAES data, respectively. Accounting for the uncompensated drift would adjust the CLAES to about 1.12.

5.1.2. 1992 to 1993 trends in the zonal mean vmr comparisons. The January 1992 and 1993 CLAES zonal means in Figure 16 show ratios of peak vmr from 1992 to 1993 of the order of 1.33, 1.42, 1.04, 1.05, and 0.84 at 32°S, 0°, 30°N, 60°N,

Table 3. Systematic Error Estimates in HNO_3 vmr

Error Source	Pressure, mbar			
	70	30	10	3
Radiometric calibration	1.8	1.4	1.9	4.5
Spectral calibration	1.1	0.8	0.6	0.6
Spectral response function	4.8	4.2	3.0	3.0
Array spectral dispersion	1.8	1.4	1.0	1.0
Detector spatial response	0.9	0.7	0.5	0.5
Optical cross talk	0.4	0.3	0.4	1.0
Spectral parameters	8.5	6.5	5.0	5.0
Temperature sensitivity	10.0	8.0	5.0	4.0
Forward radiance	1.8	1.4	1.0	1.0
RSS of errors	14.4	11.5	8.1	8.6

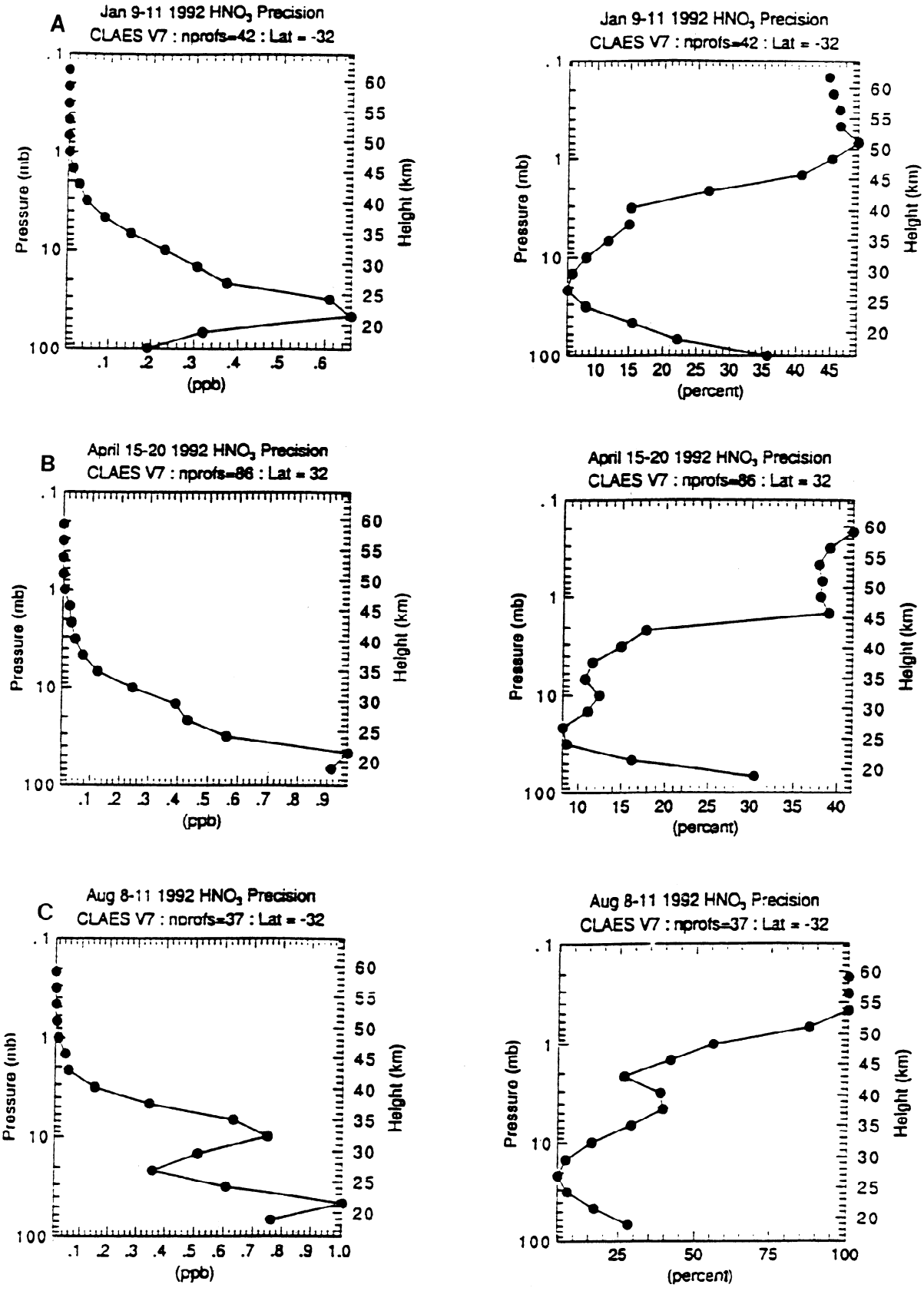

Figure 18. Precision estimates derived from turnaround data for six sets of days, including (a) 32°S for January 9–11, 1992; (b) 32°N for April 15–20, 1992; (c) 32°S for August 8–11, 1992; (d) 32°N for August 25–30, 1992; (e) 32°S for January 3–5, 1993; and (f) 32°N for April 1–3, 1993.

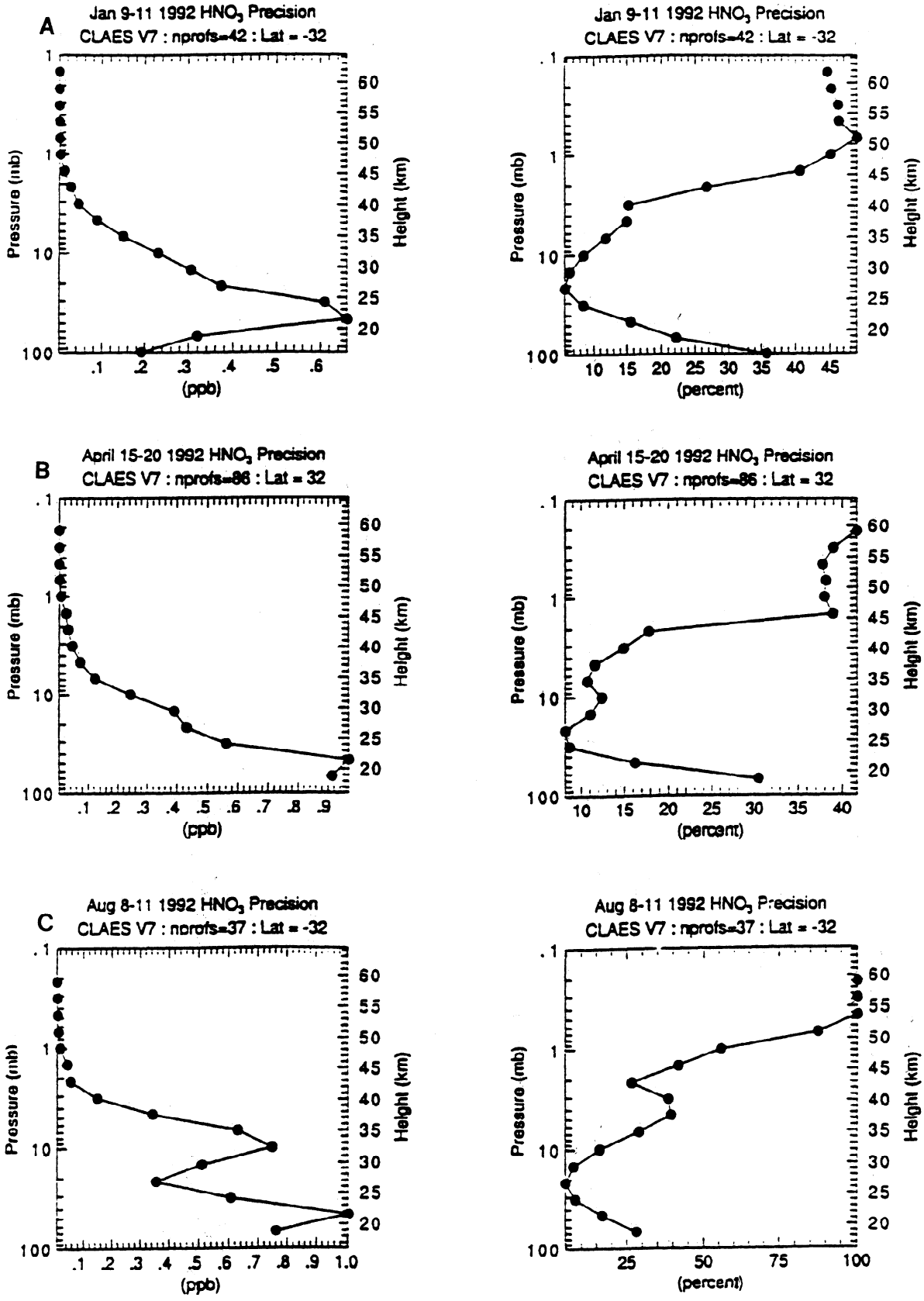

Figure 18. (continued)

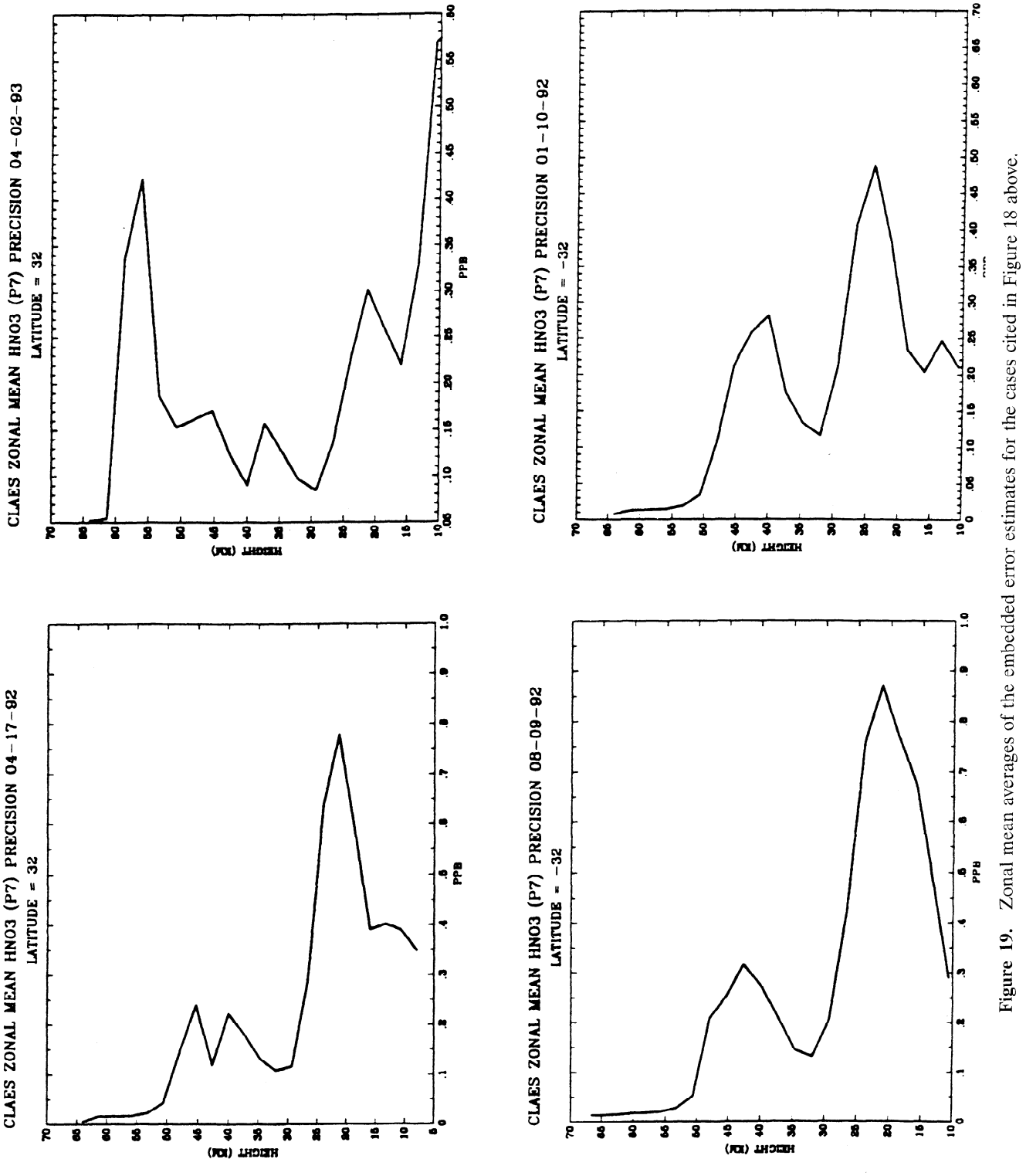

Figure 19. Zonal mean averages of the embedded error estimates for the cases cited in Figure 18 above.

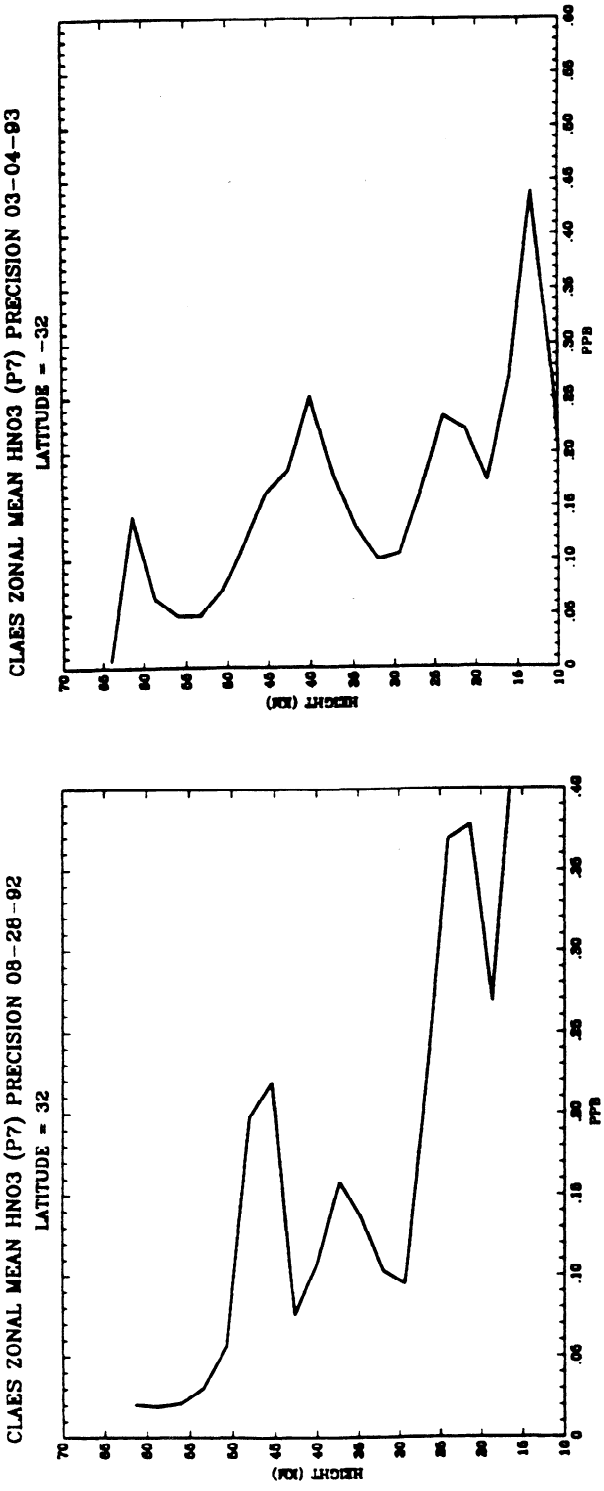

Figure 19. (continued)

and 76°N, respectively, on adjusting for uncompensated drift in radiometric calibration. The trend to decrease from 1992 to 1993 is very evident near the equator and in the south, is weak at most in the north midlatitudes, and is reversed at the highest north latitude. The LIMS is much more similar to the 1993 case indicating that of the January 3 cases, CLAES 1992 is the exception. This is true too for the April (selected to be coincident with CLAES/ATMOS comparisons) comparisons with LIMS shown in Figure 17. Here the ratios of peak vmr from 1992 to 1993 are of the order of 1.36, 1.37, 1.45, 1.69, and 1.09 at 65°S, 50°S, 30°S, 0°, and 32°N, respectively, on adjusting for uncompensated drift. For 50°S and 31°S these trends compare well with those derived from profiles coincident with ATMOS data, for both CLAES and ATMOS. It should be noted that the values 1.04 for the 30°N January trend ratio and 1.09 for the 32°N April trend ratio are both smaller than the CLAES 1.12 trend ratio derived from comparisons of profiles coincident with the FIRS-2 and the FIRS-2 1.13 trend ratio. In this comparison, more weight should be given to the zonal mean trends because these are less affected by longitudinal variation than are individual profiles; however, daily zonal means are subject to day-to-day variation. This variation in zonal mean columns is evident in data that are discussed in the following subsection.

5.1.3. Trends in HNO_3 columns. Integrated HNO_3 column data obtained at the Lauder, New Zealand, site (45°S, 170°E) from June 1990 to December 1993 have been reported by *Koike et al.* [1994] and *Jones et al.* [1994]. These show a clear trend of decrease over the set of CLAES V7 processed days. In discussion below, the data from *Koike et al.* [1994] are designated by KCD. For comparison the CLAES zonal mean HNO_3 column at 44°S and 48°S are shown in Figure 20. The CLAES data are plotted versus the day from the launch of the UARS, i.e., UARS days. For reference the UARS day 112 corresponds to January 1, 1992, and UARS day 478 to January 1, 1993. Over the CLAES mission lifetime there are seven south-looking periods (SLP) such that data at 44°S and 48°S could be obtained. Those seven SLP, the average value (AC) of the CLAES HNO_3 column for those periods for 44°S and 48°S, and the corresponding KCD values of AC (estimated at the middle of each SLP by inspection of Figure 1 in that publication) are presented in Table 5. The CLAES values are in reasonable agreement with KCD and, in particular, show a similar large enhancement [*Jones et al.*, 1994] over the seasonal norm. Deseasonalized CLAES column trend ratios can be calculated for SLP 1 to 6 since these are spaced by approximately one year, as are the SLP 2 and 7. Note that CLAES data obtained past UARS day 582 were not included in SLP 7 due to difficulties in spacecraft operations on days 583 through 587, and some reservations as to the V7 calibration procedure for the south-looking days 588 through 590 following those difficulties, and prior to door close on 591 in preparation for the yaw maneuver. The CLAES 1992 to 1993 column ratios, adjusted for the uncompensated drift in radiometric calibration, at 44°S and 48°S, i.e., the ratio of AC for SLP 1 to AC for SLP 6, are both 1.04 ± .03, and for the KCD it is estimated to be of the order of 1.06 ± 0.7. For the SLP 2 to 7 column trend ratios the adjusted CLAES values are 1.20 ± 0.06 and 1.25 ± 0.06, respectively, and the KCD ratio is estimated to be 1.11 ± 0.09. Considering the variability, the CLAES and KCD trend ratios agree for both the SLP 1 to SLP 6 and the 2 to 7 comparisons. These decreasing trends in the CLAES column are not so large as is noted in peak vmr from profile and zonal mean comparisons above, perhaps an indication the trend may be weaker at altitude below the peak vmr, which has more influence on the column.

To compare the corresponding north midlatitude trends in the period of CLAES V7 processed data, the zonal mean HNO_3 column at 44°N and 48°N is shown in Figure 21. The north-looking periods (NLP) are listed in Table 6 as are the corresponding AC and VC. Deseasonalized column trend ratios can be calculated for NLP 1 to 6 since these are spaced by approximately one year, as are the NLP 2 and 7. For 1 to 6 the

Table 4. Random Error Estimates

Error Source	Pressure, mbar 70	30	10	3
Radiometric calibration	5.0	2.7	1.7	1.7
Spectral calibration	4.5	2.5	2.0	2.0
Cold space NESR	0.3	0.3	2.0	14.0
Vertical smear	2.0	≪2.0	2.0	2.0
Horizontal gradients	4.5	2.5	2.0	2.0
Atmospheric temperature	9.0	5.0	2.0	2.0
RSS of errors	12.3	6.7	4.8	14.7

Percent HNO_3 volume mixing ratio.

values are 1.05 ± 0.04 and 1.05 ± 0.05 at 44°N and 48°N, respectively. For 2 to 7 the values are 0.94 ± 0.06 and 0.91 ± 0.07 at 44°N and 48°N, respectively. Thus consistent with the zonal mean vmr comparisons there is no clear trend of decreasing zonal mean HNO_3 column in the north midlatitudes during the period of CLAES V7 processed data. Note too that the north winter variabilities are somewhat larger than in the south, probably due to more active winter dynamics in the north.

Another HNO_3 column data set [*David et al.*, 1994] obtained from Mauna Loa, 19.51°N, in the time period mid-October 1991 to mid-October 1993 has recently been published. In this 2-year time period the column decreased by 30%. In the discussion below, the data from *David et al.* [1994] are designated by DCD. The zonal mean averaged CLAES HNO_3 column at 20°N and the DCD are plotted together on the shorter subset period of CLAES V7 processed data in Figure 22. There is good agreement in the two data sets. One year separates the period from January 9 to April 15, 1992 (UARS days 120 to 217, henceforth designated as MLP 1) at the beginning of the CLAES V7 processing period from the period January 9 to April 15, 1993 (UARS days 486 to 582, henceforth designated as MLP 2) at the end of the CLAES V7 processing. Since MLP 1 and 2 are spaced by approximately one year, the ratio of the AC for those two periods, 1.06 ± 0.04, provides a deseasonalized trend from February 26, 1992, the midpoint of MLP 1, to February 26, 1993, the midpoint of MLP 2. The corresponding deseasonalized trend ratio for MLP 1 to 2 for the DCD is 0.99 ± 0.13, consistent with the CLAES value. This obviously statistically significant, deseasonalized 6% HNO_3 decrease at 20°N during the 1-year period February 26, 1992, to February 26, 1993, is considerably slower than the average value of 15% per year that occurred in the 2-year time period from mid-October 1991 to mid-October 1993 as derived from the DCD in that time period. The corresponding trend ratio for the end of February 1992 to end of February 1993 derived from the 20°S CLAES column data is 1.24 ± 0.08. These results for the 20°S–20°N asymmetry in the decrease in HNO_3 column during the period of CLAES V7 processed data are generally consistent with what is seen in the 44°S and 48°S–44°N and 48°N case in that the column trend ratios are in the same sense as the corresponding peak vmr trend ratios but are not quite so large.

A summary of the global deseasonalized averaged zonal column trend ratios is given in Table 7 below. It is seen that in the period of CLAES V7 processed data the deseasonalized trend for decrease in HNO_3 from 1992 to 1993 is very clear and distinct in the southern hemisphere. It is not so in the north middle to high latitudes and, in fact, it is increasing, especially in that the NLP 1 consists of only 3 days and a partial day, and therefore the comparisons of the NLP 2 to 7, which indicate increasing HNO_3, should carry more weight than the comparisons of NLP 1 to 6 that indicate a small to moderate decrease. Where there are correlative data, trends in these are consistent with the CLAES trends for the time periods that are addressed, as was the case with the profile comparisons discussed above.

5.2. Trend Mechanisms

Credible trend mechanisms increase confidence in the data. The heterogeneous conversion of N_2O_5 to HNO_3 on Pinatubo aerosol has been predicted by *Hoffman and Solomon* [1989] to enhance HNO_3 in 1992 as compared to 1993. The decrease in HNO_3 in going from 1992 to 1993 would result from the diminishing influence of heterogeneous conversion of N_2O_5 to HNO_3 as the Pinatubo aerosol settles out during this time period, and the HNO_3 recovers toward pre-Pinatubo conditions. This interpretation has been applied by previous authors reporting HNO_3 trend observations [*Rinsland et al.*, 1994; *Jones et al.*, 1994; *Koike et al.*, 1994; *David et al.*, 1994]. This is a strong candidate mechanism to explain the globally averaged deseasonalized trends of decreased HNO_3 column and peak vmr on going from 1992 to 1993 that is observed by the CLAES instrument. Consistent with this mechanism for explanation of the decrease in HNO_3 the CLAES data indicate a corresponding strong 1992 to 1993 global decrease in the Pinatubo aerosol [*Mergenthaler et al.*, 1992; *Roche et al.*, 1994; *Massie et al.*, this issue]. In the following discussion we will refer to this mechanism as the recovery from the HNO_3 enhancement due to Pinatubo aerosol surface conversion of N_2O_5 to HNO_3, i.e., the rfPac mechanism.

However, clear evidence for decrease in HNO_3 from 1992 to 1993 for the period of CLAES V7 processed data is restricted to the latitude 30°N and south. Since to first order we expect the decrease in HNO_3 due to the rfPac to be uniform over the globe, and especially since it is very unlikely the rfPac can produce increased HNO_3 as observed in the northern deseasonalized CLAES HNO_3 trends, the observations suggest

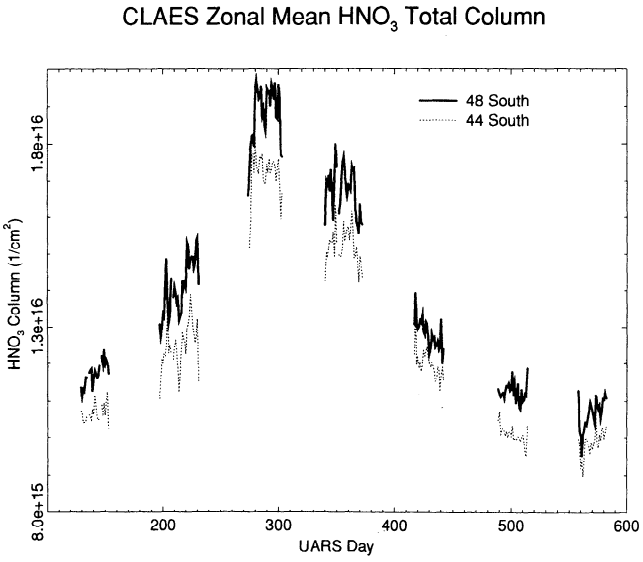

Figure 20. Mission length time series of CLAES HNO_3 zonal mean column density at 44°S and 48°S. UARS day 112 corresponds to January 1, 1992, and UARS day 478 to January 1, 1993.

Table 5. Details of Comparison With KCD

Number	SLP	UARS Days	CLAES 44°S		CLAES 48°S		KCD	
			AC	VC	AC	VC	AC	VC
1	Jan. 17–Feb. 12, 1992	128–154	10.6	0.2	11.7	0.3	12.2	0.8
2	March 26–April 29, 1992	197–231	12.5	0.6	14.1	0.7	13.9	1.0
3	June 11–July 10, 1992	274–303	17.2	0.5	18.9	0.7	19.1	1.7
4	Aug. 16–Sept. 18, 1992	340–373	15.2	0.5	16.7	0.6	17.0	1.2
5	Nov. 1–26, 1992	417–442	11.9	0.3	12.8	0.4	11.4	0.8
6	Jan. 12–Feb. 6, 1993	489–514	10.1	0.2	11.2	0.2	11.5	0.3
7	March 22–April 15, 1993	558–582	9.9	0.3	10.7	0.4	12.5	0.7

The south-looking period (SLP) averaged zonal HNO_3 column (AC) and its variability (VC) in units 10^{15} cm^{-2} is listed for CLAES, and estimates (as discussed in text) for the KCD HNO_3 column at the middle of each period, and its variability.

that there is an additional mechanism for the observed deseasonalized trends in the CLAES HNO_3. Also, there is a much larger decrease of HNO_3 column at 20°S compared to 20°N and at the equator; this suggests that the additional mechanism may have influence on HNO_3 column as far south as the equator. This additional mechanism must act to increase HNO_3 during the time periods of the deseasonalized trends, approximately from February 1992 to February 1993, but not necessarily fast enough at all latitudes in these regions to totally offset the decrease in HNO_3 due to the rfPac.

It is interesting and relevant to examine the implications for this additional mechanism of the 20°N DCD and CLAES data. The corresponding aerosol surface area from SAGE (monthly mean values integrated from 10° to 20°N and from 15 to 35 km) in the time period mid-October 1991 to mid-October 1993 is also shown by *David et al.* [1994] and cited (G. Yue, private communication, 1994). The maximum aerosol surface area occurs at approximately the end of December 1991 and is approximately 400 μm^2 km/cm^3. The aerosol surface areas are 360 and 70 μm^2 km/cm^3 for February 26, 1992, and February 26, 1993, respectively. So, in the 1-year time period from February 26, 1992, to February 26, 1993, that the aerosol decreases by a factor of more than 5 from February 26, 1992, and by more than a factor of 4 from peak loading near the end of December 1991, the HNO_3 column only decreases by 6%, which constitutes just one fifth of the total 30% that it decreased in the 2-year period from mid-October 1991 to mid-October 1993. To reiterate, more than 75% of the maximum that occurred in Pinatubo-enhanced aerosol surface area settles out in the time period from February 26, 1992, to February 26, 1993, but only one fifth of the total decrease in HNO_3 that is noted from mid-October 1991 to mid-October 1993 occurs in that same time period. The other four fifths of the total 2-year HNO_3 decrease occurs in the two time segments from mid-October 1991 to February 26, 1992, and from February 26, 1993, to mid-October 1993. At 20°N the decrease in HNO_3 and aerosol certainly does not track one to one.

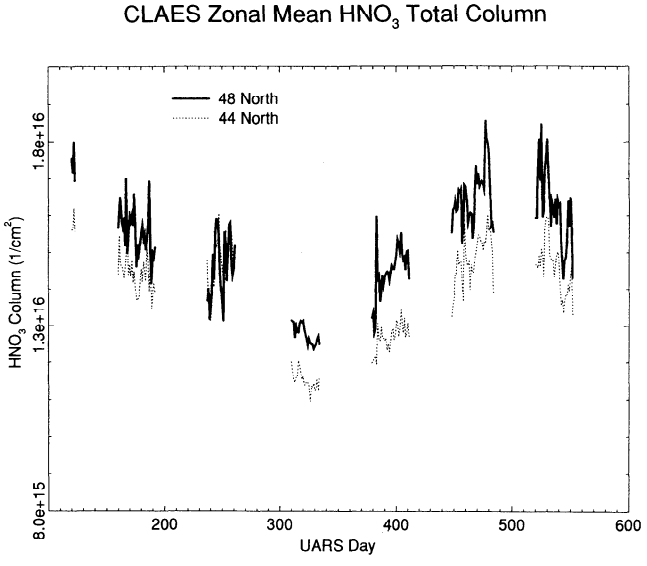

Figure 21. CLAES HNO_3 zonal mean column density at 44°N and 48°N.

On the other hand, at 20°S there is a 25% decrease noted in the CLAES data (section 5.1.3 above) during the major aerosol dispersal time period from February 26, 1992, to February 26, 1993. This behavior at 20°S is what might be expected at 20°N if the decrease in HNO_3 were to track one to one with the settling out of the aerosol. To satisfy the DCD requirement for a 30% decrease at 20°N in the 2-year period from mid-October 1991 to mid-October 1993, and to also satisfy the CLAES (and DCD requirement) requirement that only 6% of this decrease occurs in the one year from February 26, 1992, to February 26, 1993, which also happens to be the specific time in which more than 75% of the aerosol surface area settles out, the postulated additional mechanism is required to produce only a transient effect. It is required to tend to increase HNO_3 in the approximate time period February 1992 to February 1993 but not outside this time period. At 20°N the effect is required to be significant but not strong enough to totally offset the decrease in HNO_3 column due to the rfPac. To explain the hemispheric asymmetry evident in Table 7 and to be consistent with trends common to CLAES and ATMOS in the southern hemisphere as derived from profile comparisons, the mechanism must be operative in the sense that it would drive increases in HNO_3 from the equator and to the north but should not be operative in this sense to the south of the equator.

The QBO is a plausible candidate for this additional mechanism. A large variation has been predicted in HNO_3 [*Chipperfield and Gray*, 1992] and prior to significant processing of the UARS data, *Gray and Ruth* [1992] predicted HNO_3 QBO effects in the UARS data with magnitude and timing comparable to the CLAES observations for the hypothetical case of no Pinatubo eruption. Considering these predictions and the magnitude of the observed effects, it is reasonable that the QBO may be exerting significant influence. If the additional mechanism is QBO related it must have considerable hemispheric asymmetry to meet the requirements on the proposed additional trend mechanism. As discussed above, it

Table 6. As Listed in Table 5 but for 44°N and 48°N

Number	NLP	UARS Days	CLAES 44°N		CLAES 48°N	
			AC	VC	AC	VC
1	Jan. 9–12, 1992	120–123	15.8	0.3	17.4	0.4
2	Feb. 18–March 21, 1992	161–192	14.4	0.4	15.5	0.6
3	May 4–30, 1992	236–262	14.8	0.8	14.8	0.8
4	July 16–Aug. 10, 1992	309–334	11.5	0.2	12.7	0.3
5	Sept. 24–Oct. 26, 1992	379–411	12.7	0.3	14.5	0.6
6	Dec. 2, 1992, to Jan. 7, 1993	448–484	14.9	0.6	16.5	0.7
7	Feb. 12, 1992, to March 17, 1993	520–553	14.5	0.7	16.1	1.0

would need to be working to increase HNO_3 peak vmr from about 30°N and to the north and HNO_3 column from about the equator and to the north on the approximate time period from February 1992 to February 1993. To the south of these regions it is required to either have little effect or to be driving a decrease in HNO_3, i.e., in the same sense as the rfPac.

Hemispheric asymmetry is observed in NO_2 QBO signals in SAGE data on the time span from 1985 to 1991 [*Chipperfield et al.*, 1994] and rationale is presented. The HNO_3 QBO signals are expected to resemble those in NO_2 [*Chipperfield and Gray*, 1992]. Also, hemispherically asymmetric behavior is noted in the MLS ozone data [*Froidevaux et al.*, 1994] in the time period concurrent with the CLAES data. These are seen most clearly in the MLS column ozone above 100 mbar (*Froidevaux et al.* [1994], Figure 7a; these are designated by MLS · $O_3C_{>100}$ in subsequent discussion) that show deseasonalized trends that are very similar to those seen in the CLAES HNO_3 data. The MLS has the same viewing geometry as CLAES, so periods defined above for establishing deseasonalized trends are common to the two UARS instruments. From 15°N to 80°N there is a decreasing deseasonalized trend in MLS · $O_3C_{>100}$ from NLP 1 to NLP 6 and from NLP 2 to NLP 7, an increasing deseasonalized trend from MLP 1 to MLP 2 from 15°N to 15°S, and no significant trend from 15°S to 80°S for SLP 1 to SLP 6 and SLP 2 to SLP 7. The MLS has obtained data over a longer time base than CLAES, and the data available for the [*Froidevaux et al.*, 1994] publication went from October 1991 to mid-March 1994. On examination of that total data set it is clear that the deseasonalized trends in the MLS · $O_3C_{>100}$, as described above, exhibit the characteristics of QBO extrema with maximum in the north occurring at about February 1, 1992, minimum occurring at about February 1, 1993, and another maximum occurring at about February 1, 1994. The identification is even clearer in the 15°N to 15°S region where the phasing is reversed by 180° as models would predict for the ozone QBO signal. Similar QBO phasing and hemispheric asymmetry is also apparent [*Froidevaux et al.*, 1994] in a comparison of MLS and TOMS total ozone column from 30°N to 60°N and from 30°S to 60°S, although the asymmetry is not so pronounced in these data.

The QBO-like behavior required for the additional mechanism for the deseasonalized trends that are observed in CLAES HNO_3 peak vmr would need to be 180° out of phase with the QBO-like signal in the MLS · $O_3C_{>100}$ on the range from 15°N to 80°N. This is consistent with models of the QBO effects on ozone, NO_2, and HNO_3. It is expected that the CLAES HNO_3 peak vmr is ≈180° out of phase with the MLS · $O_3C_{>100}$ on the rest of the globe too, but it would be difficult to clearly distinguish this in the deseasonalized trend data since it would drive toward decreasing HNO_3, the same sense as the rfPac. In the case of the deseasonalized trends in CLAES HNO_3 column the QBO-like effects in the north again need to be 180° out of phase with those observed in MLS · $O_3C_{>100}$ in the range from 15°N to 80°N but would need to have this behavior on the somewhat larger region from the equator to 80°N in order to explain the hemispheric asymmetry observed in these as listed in Table 7 above.

Also, QBO-like behavior in HNO_3, with minimum in approximately February 1992 and maximum in approximately February 1993, is exactly what is needed to simultaneously explain the observation of the relatively slow 6% deseasonalized decrease seen (section 5.1.3) in 20°N HNO_3 column data from February 1992 to 1993, which is just a small fraction of the 30% decrease in 20°N HNO_3 column data that is observed [*David et al.*, 1994] in the inclusive 2-year period from October 1991 to 1993. Because of its 2-year period the QBO should have little influence on the 30% trend noted in the DCD from October 1991 to 1993. This should be driven nearly exclusively by the rfPac. But QBO-like phasing with minimum in approximately February 1992 and maximum in approximately February 1993, as proposed, is exactly what is required to provide consistency of the 2-year 30% trend to decrease with the much slower 6% trend to decrease that is observed in the shorter deseasonalized subset period from February 1992 to 1993. Assuming the rfPac drives a 15% decrease per year, the peak-

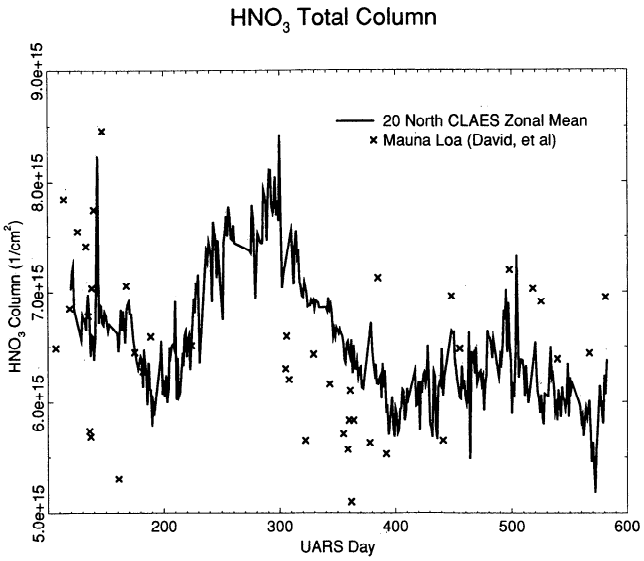

Figure 22. A comparison of the CLAES HNO_3 zonal mean column density at 20°N and the data from *David et al.* [1994].

Table 7. Summary of Deseasonalized Average Column Trend Ratios for Decrease in HNO_3 for 1992/1993

Latitude, deg	South			North		
	SLP 1 to 6	SLP 2 to 7	MLP 1 to 2	NLP 1 to 6	NLP 2 to 7	MLP 1 to 2
76	1.05	1.21		1.15	0.91	
60	1.05	1.30		1.02	0.93	
48	1.04*	1.25*		1.05	0.91	
44	1.04*	1.20*		1.05	0.94	
20			1.24			1.06†
0			1.07			

*Consistent with data from *Koike et al.* [1994].
†Consistent with data from *David et al.* [1994].

to-peak QBO-like effect that is required to match the observations is a 9% increase.

Considering the discussion above, it is solidly plausible that the QBO may be the additional mechanism that is required to fit the observed deseasonalized CLAES HNO_3 trends in that the hemispheric asymmetry and timing of the extrema are consistent with the concurrently observed QBO-like signals in MLS data, the required magnitude of the effect is consistent with models, and the timing and magnitudes explain the time dependence of the CLAES and DCD trends observed in the 20°N HNO_3 column data. These are strong plausibility arguments in support that the required second mechanism for the observed 1-year deseasonalized trends is a QBO effect with characteristics as proposed above but perhaps just short of being conclusive. A more extensive study is required which involves the identification of concurrent QBO-like signals in other species (CLAES · $O_3C_{>100}$ and MLS HNO_3 are obvious examples) and the use of models to see if these are consistent with the required effects on HNO_3. Such a study is out of scope for this validation paper.

Our conclusions on mechanisms for the deseasonalized trends observed in the CLAES HNO_3 on the time period of V7 processed data are as follows:

1. Averaged over the globe, there is a decrease in HNO_3 that is most likely dominated by the diminishing influence of heterogeneous conversion of N_2O_5 to HNO_3 as the Pinatubo aerosol settles out and the HNO_3 tends to recover toward ambient pre-Pinatubo levels, as has been discussed by previous authors.

2. There is, however, a strong hemispheric asymmetry in that the HNO_3 decrease is very clear and distinct in the south, is relatively weakly present in the north subtropics, and is not present, or actually reversed at northern middle and high latitudes. This suggests the existence of a second trend mechanism that significantly influences the observed trend data.

The QBO is a strong candidate for this second mechanism. The required timing and hemispheric asymmetry is consistent with the QBO-like signals reported for the MLS O_3 column above 100 mbar and model-predicted effects are of the required magnitude.

5.3. Data Usage Caveats

The comparison with correlative data presented above shows a picture of CLAES HNO_3 V7 values that are generally less than the corresponding correlative data for cases where CLAES peak vmr are approximately ≤8 ppbv. In these cases the use of the most recent spectral parameters, as will be done in future data versions, is expected to improve the comparisons with correlative data. For cases where the CLAES peak vmr exceeds 10 ppbv there is no evidence that these are smaller than the corresponding correlative data; therefore in these cases the use of the most recent spectral parameters is not expected to improve the comparisons with correlative data.

There are two cases where the CLAES average peak vmr exceeds 10 ppbv in comparison with a set of correlative profiles; these are the ATMOS 92 sunset and the CAESR profiles. The CLAES average peak vmr in these two cases is 10.25 and 12.0 ppbv, respectively. The average value in the difference of peak vmr for these two cases is 7 ± 11% and 7 ± 10%, respectively. Thus for CLAES profiles with peak vmr greater than 10 ppbv, these are somewhat larger on the average than in the correlative profile set but are well within the variability. In addition to the profile comparisons, there are two other cases we have examined that indicate CLAES is achieving retrievals in agreement with correlative data for peak volume mixing ratios well in excess of 10 ppbv. The good agreement of the CLAES column data with the KCD in the same time period, SLP 2, and approximate location of the comparisons with the ATMOS 92 sunset data, and the continued good agreement with KCD in the next time period, SLP 3, in that location when the amount of HNO_3 was increased by about 35%, would argue that at least up to this amount of HNO_3 the CLAES is retrieving consistent with correlative data. Also, direct comparison with CLAES polar HNO_3 mapped on the 465 K surface as shown by *Roche et al.* [1994, Figure 2] for the dates October 26, 1992, December 3, 1993, February 22, 1992, and March 14, 1993, with similar mapped MLS data for these dates, as shown by *Santee et al.* [1995, Figure 2], demonstrate that the CLAES data consistently portray the morphology for vmr that exceeds 13 ppbv.

The following is a summary of the caveats:

1. The spectral parameters that were used in V7 are now out of date. The most recent parameters will be incorporated in the next CLAES data version and are expected to increase the retrieved vmr by about 10% in optically thin regions and by as much as 25% in the optically thickest regions.

2. The CLAES V7 HNO_3 with peak vmr ≤8 ppbv are on the average 6–15% smaller than the peak vmr in available correlative profiles. These comparisons are expected to improve with the use of the most recent spectral parameters since this is expected to increase the CLAES by 10–16% in these cases.

3. On the basis of profile comparisons with correlative profiles the CLAES V7 HNO_3 with peak vmr ≥10 ppbv are more than correlative profile peak vmr by about 7 ± 11%. Comparison with KCD and published mapped MLS data indicate agreement within variability is retained to vmr at least as large as 13 ppbv. The use of new spectral parameters in future

versions might be expected to produce an increase in the CLAES values for these cases of large HNO_3.

4. Beginning August 10, 1992, there is an uncompensated drift in the V7 radiometric calibration that produces a decreasing bias in CLAES V7 HNO_3 that goes approximately linearly from 0% on August 10, 1992, to 0.6% on January 7, 1993, then begins to decrease even more rapidly to a minimum of 3.7% too low on April 4, 1993, and then recovers by April 24, 1993. The maximum effect on vmr occurs on April 4, 1993, and tends to bias values too low by approximately 6.3, 5.2, 3.7, and 3.7% at 70, 30, 10, and 3 mbar, respectively.

6. Summary and Conclusions

There are 388 days of CLAES V7 HNO_3 global data interspersed in the period from January 9, 1992 to May 5, 1993. The most interesting science aspects of these new data are twofold. First, they provide a global view of the autumn-winter-spring evolution of the denitrification event at south high latitude, an essential element of the dramatic ozone reduction in that region in the spring. Second, the data were obtained during a period when the atmosphere was recovering from effects of the heavy Pinatubo aerosol loading, and they lend critical insight on the relative magnitude of the transient aerosol effects on comparison with other, more permanent mechanisms for year-to-year variability, the QBO for example. In this report we have examined the quality of these data. These have been compared with correlative vmr profiles, LIMS data, column data time series, and some published mapped data. Accuracy and precision are inferred from the comparisons and these are consistent with estimates that are based on instrument and retrieval characterization. One-year deseasonalized trends with considerable hemispheric asymmetry are strikingly evident in the data. These are quantitatively supported by correlative data in all cases in which these are available for suitable time periods in a given location. These are documented and credible trend mechanisms are established.

Profile comparisons were made with concurrent correlative measurements obtained by ATMOS in late March-early April 1992 and in early April 1993; 11 profiles were obtained by various instrumentation on midlatitude balloons (approximately 35°N) and interspersed in time near the equinoxes, spring and summer, and 6 northern (approximately 68°N) winter profiles from balloons. In 1992 there were 17 sunset ATMOS profiles in the range from 31.8°S to 55.5°S, 21 sunrise profiles from 16.7°S to 18.2°N, and in 1993 only 14 sunset profiles were concurrent and these were from 27.4°S to 49.5°S. Registration versus the balloon profiles and the ATMOS 92 sunset case is within 0.4 km. The registration offset is larger for the ATMOS 92 sunrise and ATMOS 93 sunset cases in which very fewer profiles were processed to low enough altitude to be used for registration purposes. A good peak vmr agreement is achieved in all cases. The CLAES values tend to be less than correlative for cases where the CLAES peak vmr is approximately $\leq$8 ppbv. In all these cases, namely, ATMOS 92 sunrise, ATMOS 93 sunset, and midlatitude balloons, agreement within variability is just missed. Conversely, for CLAES peak vmr approximately $\geq$10 ppbv the tendency is for the CLAES values to be slightly larger than correlative but to agree within variability. At both 70 and 10 mbar the CLAES vmr agrees within variability with the balloon measurements. For the most part, agreement within variability is achieved with ATMOS; the variabilities are larger than in the case of the balloon comparisons. From 10 to 3 mbar the large majority of the data points from midlatitude balloons agreed within the combined instrumental error estimate, the majority of comparisons with ATMOS were within variability, and there were no high-latitude balloon data in this altitude range. There were five midlatitude balloon profiles down to 100 mbar and, on the average, CLAES was less by 24 $\pm$ 35%. None of the midlatitude profiles went lower than 119 mbar. At high latitude it was possible to compare three profile pairs at 100 mbar and there CLAES was less, on the average, by 33 $\pm$ 10%.

Zonal Mean vmr Comparison With LIMS

These comparisons show good agreement in overall structure and in subtle features such as polar winter enhancements above 10 mbar and poleward from 50°. These comparisons for January and April showed LIMS values in the tropics and south in much closer agreement with the 1993 case. Closer agreement between the LIMS and the 1993 CLAES, rather than the CLAES 1992, is predicted by *Gray and Ruth* [1992] on the basis of QBO phasing. As in comparison with some of the correlative profiles above, the CLAES top and bottom side vertical gradients are steeper than LIMS.

Vmr Accuracy and Precision

Our highest confidence for the CLAES HNO_3 V7 vmr is in the range 70 to 3 mbar, with comparison with correlative data as summarized in Table 2 above. Although the few comparisons at 100 mbar are also very encouraging, caution should be exercised for use outside this range. The precision in the range 70 to 3 mbar is of the order of 0.3 to 1.0 ppbv. This precision was derived from data repeatability. The embedded error estimates and the estimates based on instrument and retrieval characterization agree within a factor of 2 or better.

Zonal Mean Column Comparisons

Comparisons over the time period of the CLAES V7 processed data with long time series column data reported by *Koike et al.* [1994] and *David et al.* [1994] at 45°S and 20°N, respectively, were in agreement within data variability.

Caveats

There are two important caveats regarding the CLAES V7 data. First, the V7 is biased low due to use of now out of date spectral parameters. This is estimated to be of the order of 10 to 25% with the latter number applicable for the most optically thick regions. The manifold comparisons suggest that in cases where peak V7 vmr is approximately $\leq$8 ppbv, then adjustment for spectral parameters will improve the comparisons. For peak V7 vmr from about 10 to 13 ppbv however, good agreement is achieved over the manifold comparisons, and this might be degraded on adjustment for spectral parameters. Future versions of CLAES HNO_3 data will use the most recent spectral parameters. Second, the V7 are further biased slightly low on a restricted time period due to an uncompensated drift in radiometric calibration that begins August 10, 1992, and increases slowly to values of about 1% or less on January 7, 1993, and then more rapidly to maximum values of 6.3, 5.2, 3.7, and 3.7% at 70, 30, 10, and 3 mbar, respectively, on April 4, 1993, and then recovers by April 24, 1993. Even with these caveats the HNO_3 V7 database will support a wide range of very useful science investigations, denitrification and trends being a subset of examples.

Observations of Deseasonalized Trends and Their Mechanisms

The CLAES V7 data period of processed data included January 9 through April 15 of both 1992 and 1993. Data obtained in a group of days, or on a day, within the 1992 period were compared with data obtained in the corresponding group of days, or day, within the 1993 period to examine 1-year deseasonalized trends in the data. There is an obvious trend for the southern hemispheric and equatorial HNO_3 to decrease in going from 1992 to the corresponding time in 1993. The decreasing trend is not globally universal, it is reversed for north middle and high latitudes. The decreasing trends in the south are larger than increases in the north, so that the global average is a decrease. We believe that the mechanism for the global averaged decrease is the result of the diminishing influence of heterogeneous conversion of N_2O_5 to HNO_3 as the Pinatubo aerosol settles out during this time period and the HNO_3 recovers toward pre-Pinatubo conditions (designated the rfPac mechanism in section 5.2). We believe the increase in the north is the result of hemispherically asymmetric QBO-like effects that are strong in the northern hemisphere and weak in the southern hemisphere and are phased to produce an increase in HNO_3 over this time period of just the right magnitude to more than offset decrease due to the rfPac. We have noted similar QBO-like effects with consistent phasing and hemispheric asymmetry in the concurrent MLS column ozone above 100 mbar [*Froidevaux et al.*, 1994], and various authors, as cited in section 5.2, have predicted QBO HNO_3 effects with the required magnitude.

Appendix A: CLAES V7 Approach for Retrieval and Embedded Error Estimates

A1. Introduction

In this appendix we describe the CLAES V7 approach for retrieval and embedded error estimates in application for the retrieval of HNO_3. As described by *Roche et al.* [1993a], the CLAES instrument uses order sorting blocker filters to isolate spectral regions with prominent emission features of one or more species of interest for upper atmospheric dynamics and chemistry. Aerosol emission is also present in all these blocker filter transmission regions. The blocker filters transmission passbands full width at half maximum $\Delta\lambda_B$ are typically of the order of 0.5% λ (or $\Delta\nu_B$ is of the order of 0.5% ν if we refer to spectral position in wave numbers per centimeter as is done for the most part in the CLAES validation papers). The etalon full width at half maximum bandwidths $\Delta\nu_e$ are of the order of 1/20 to 1/30 of $\Delta\nu_B$; that is, the finesse is of the order of 20 to 30 for the CLAES etalons. However, as explained by *Roche et al.* [1993a], due to limitations on sampling time when running the main CLAES instrument science mode, only several measurements at resolution $\Delta\nu_e$ are obtained on each interval $\Delta\nu_B$. The measurement spectral positions of the CLAES blocking filter transmission maxima and the positions within these that are sampled at etalon resolution $\Delta\nu_e$ are tabulated by *Roche et al.* [1993a].

By inspection of the tabulation it can be seen that the CLAES retrieval process involves multiple channels and multiple emitters on each blocker region. For the region near 879 cm^{-1} that is targeted for HNO_3, the retrieval is executed for the two emitters HNO_3 and aerosol, but there are four channels utilized for the measurements as shown in Table 1 in the main text. The positions of the channels in relation to the features on the CLAES mode 3 continuous spectra are shown in Figure 1 in the main text. In these channels there are also weak contributions from the emitters H_2O and CO_2, but these are modeled and their calculated radiance contributions subtracted from the data. In the remainder of this appendix we describe the CLAES V7 approach for retrieval and embedded error estimation using the HNO_3 region and channels as an example.

A2. Radiance Component $R_{\nu zj}$ Calculation for Species j at Tangent Altitude z and for Instrumental Etalon-Blocker Transmission Function $\Phi(\nu - \nu')$ Centered at Wave Number ν

The radiance that is calculated along the limb-viewing line of sight tangent at altitude z and at the etalon tilt angle position that centers the etalon transmission spike at ν will be designated $R_{\nu z}$. There are four such etalon positions (i.e., channels centered at ν) used for HNO_3 blocker filter region, for example. The radiance $R_{\nu z}$ produced by J emitting species is given by the integral along the limb view path

$$R_{\nu z} = \int d\nu' \Phi(\nu - \nu') \int B_{\nu'}\, d\tau_{\nu'}. \tag{A1}$$

where the spectral transmittance along the path is a product of the transmittances $\tau_{j\nu'}$ of the J species and is given by $\tau_{\nu'} = \Pi_{j=1}^{J} \tau_{j\nu'}$, the spectral blackbody radiance $B_{\nu'}$ is a function of temperature T along the path, and $\Phi(\nu - \nu')$ is the instrumental spectral response for transmission through all instrumental elements, including the tilted etalon and the order sorting filter, and for incidence on reflective instrumental elements.

At tangent altitude z the species component radiances $R_{\nu zj}$ are given by

$$R_{\nu zj} = \int d\nu' \Phi(\nu - \nu') \int B\, d\tau_{j\nu'}.$$

The $R_{\nu zj}$ is the radiance that would be due to specie j as if it were the only specie present in the atmosphere. Then $R_{\nu z}$ is given by the sum of the species component radiances minus an overlap term we call $L_{\nu z}$; that is,

$$R_{\nu z} = \sum_{j=1}^{J} R_{\nu zj} - L_{\nu z}. \tag{A2}$$

In practice, one calculates the $R_{\nu z}$ and the $R_{\nu zj}$ and then computes $L_{\nu z} = \Sigma_{j=1}^{J} R_{\nu zj} - R_{\nu z}$.

The use of the $R_{\nu zj}$ and $L_{\nu z}$ in the retrieval process with emphasis on describing the approach for calculating the CLAES V7 algorithmic error estimates are illustrated here for the HNO_3 case. In this region $J = 4$, the emitters are HNO_3 ($j = 1$), aerosol ($j = 2$), and weak contributions from H_2O ($j = 3$) and CO_2 ($j = 4$).

A3. Fitting Data in Multiple Channels by Multiple Species for All Tangent Altitudes z, in Effect "Diagonalizing" the Multichannel, Multiemitter Problem into a Set of Equivalent Uncoupled "Single-Channel", Single-Emitter Problems

For our example we model the H_2O and CO_2 atmospheric vmr based on climatology and retrieve the HNO_3 and aerosol. Thus the calculated radiance component due to H_2O and CO_2 is subtracted from the radiance data. Since these components

contribute only a very small amount to total radiance, the error in using climatology to model them is second order. At each tangent altitude z for the four channels denoted by $\nu = 1$–4, the HNO_3 radiance component $R_{\nu z1}$ and the aerosol radiance component $R_{\nu z2}$ that are calculated from the initial guess trial atmosphere are linearly fit to the data $D_{\nu z}$, with the H_2O and CO_2 modeled radiances $R_{\nu z3}$ and $R_{\nu z4}$ and the overlap term $L_{\nu z}$ subtracted from it; that is, the HNO_3 and aerosol radiances are best linear least squares fit to $D'_{\nu z} = D_{\nu z} - L_{\nu z} - R_{\nu z3} - R_{\nu z4}$. Mathematically, this amounts to solving for the coefficients b_{z1} and b_{z2} that minimize the quantity σ_z^2 defined below by

$$2\sigma_z^2 = \sum_{\nu=1}^{4} (D'_{\nu z} - b_{z1}R_{\nu z1} - b_{z2}R_{\nu z2})^2 \qquad \text{(A3)}$$

For the first guess for HNO_3 and aerosol the b_{zi} (here we switch notation to designate retrieved species by i; in this example $i = 1$ for HNO_3 and $i = 2$ for aerosol) are not generally unity. The least squares fitting procedure for finding the coefficients b_{zi} and the uncertainties σ_{bzi} in these coefficients is discussed by *Kumer and Mergenthaler* [1991].

To briefly review the calculation of the σ_{bzi} for the general case where I species radiance components $R_{\nu zi}$ are being fit to data in N channels by solving for the coefficients b_{zi} that minimize σ_z^2 as given below

$$(N - I)\sigma_z^2 = \sum_{\nu=1}^{N} \left(D'_{\nu z} - \sum_{i=1}^{I} b_{zi}R_{\nu zi} \right)^2,$$

The uncertainties σ_{bzi} in the fitting coefficients b_{zi} are estimated by

$$\sigma_{bzi}^2 = \sigma_z^2 C_{zii}^{-1}$$

where C_{zii}^{-1} is the diagnol element of the inverse of the least squares covariance matrix C_z that has the elements $C_{zij} = \Sigma_{\nu=1}^{N} R_{\nu zi}R_{\nu zj}$.

The retrieval process is used to modify the trial atmosphere in an iterative way to obtain the best fit to the data and thereby to drive the coefficients b_{zi} sufficiently close to unity to terminate the process. Typically, this occurs when successive iterations produce very small change when compared versus uncertainty estimates in the retrieved parameters, computed as described below in this appendix.

To illustrate, the progression of driving the HNO_3 q-branch trial radiances to fit the data, corresponding to the iterations for HNO_3 that are shown in Figure 2 of the main text, are shown here in Figure A1.

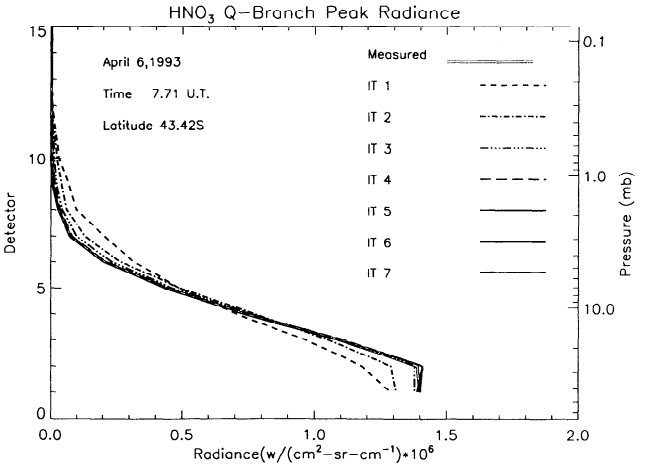

Figure A1. Illustration of iterative process driving trial radiances to observed radiances in the q-branch channel for the same case as shown in Figure 2 in the main text.

A4. Linearization and Normalization to Employ Method Resembling Single-Channel, Single-Emitter Newtonian Iterative Approach for Error Estimation and Retrieval

The calculation of $R_{\nu zi}$ can be linearized and a normalized k matrix defined by $k_{\nu zz'i} = (\partial R_{\nu zi}/\partial X_{z'i})(X_{z'i}/R_{\nu zi})$. This can be used in an approach similar to the Newtonian iterative approach that is described by *Rodgers* [1976] to iteratively drive the atmosphere to a solution and/or provide error estimates.

Linearization is achieved by using the first term of the Taylor expansion of $R_{\nu zi}$ about $R_{\nu zi}^{(n)}$, the nth iterative calculation of the component radiance; that is,

$$R_{\nu zi} = R_{\nu zi}^{(n)} + (\partial R_{\nu zi}/\partial X_{z'i})(X_{z'i} - X_{z'i}^{(n)}) \qquad \text{(A4)}$$

To describe the iterative scheme, it is convenient to utilize the radiance fitting coefficients b_{zi}, as discussed above, and to define the species modification coefficients a_{zi} as follows:

The radiance fitting coefficients b_{zi} relate $R_{\nu zi}$ and $R_{\nu zi}^{(n)}$ by $R_{\nu zi} = b_{zi}R_{\nu zi}^{(n)}$; therefore

$$R_{\nu zi} - R_{\nu zi}^{(n)} = (b_{zi} - 1)R_{\nu zi}^{(n)}. \qquad \text{(A5)}$$

Likewise, the species modification coefficients a_{zi} can be defined such that $X_{z'i} = a_{z'i}X_{z'i}^{(n)}$; therefore

$$X_{z'i} - X_{z'i}^{(n)} = (a_{z'i} - 1)X_{z'i}^{(n)} \qquad \text{(A6)}$$

Dividing both sides of (A4) by $R_{\nu zi}^{(n)}$ and rearranging gives the linearized and normalized equation

$$(b_{zi} - 1) = \sum_{z' \geq z} k_{\nu zz'i}(a_{z'i} - 1) \qquad \text{(A7)}$$

Here $k_{\nu zz'i} = (\partial R_{\nu zi}/\partial X_{z'i})(X_{z'i}^{(n)}/R_{\nu zi}^{(n)})$. The b_{zi} are determined by linear least squares fitting the radiance components to the data, as described above. The species modification coefficients $a_{z'i}$ are the unknowns that are to be solved.

There are as many linearized equations as there are channels; four for our example here applied to the region near 879 cm^{-1} for HNO_3 and aerosol retrieval. By defining a k matrix that is a weighted sum over the four channels, i.e., $k_{zz'i} = \Sigma_{\nu=1}^{4} w_{\nu i}k_{\nu zz'i}/\Sigma_{\nu=1}^{4} w_{\nu i}$, the four equations for the four channels are reduced to a single equation

$$(b_{zi} - 1) = \sum_{z' \geq z} k_{zz'i}(a_{z'i} - 1) \qquad \text{(A8)}$$

We have not investigated what constitutes optimized weighting factors. For the V7 data we have used the weighting factors $w_{\nu i} = \Sigma_z (k_{\nu zzi}R_{\nu zi}/\mathrm{NESR}_{\nu z})^2$ where $\mathrm{NESR}_{\nu z}$ is the noise equivalent spectral radiance in channel ν at altitude z. The $\mathrm{NESR}_{\nu z}$ are derived by fitting a model to data obtained during on-orbit CLAES door closed blackbody cool down calibration events, as described by *Roche et al.* [1993a]. For the long wave channels the door never gets cold enough that the blackbody radiance is equal to the higher-altitude atmospheric radiance. For these cases the $\mathrm{NESR}_{\nu z}$ derived from the cool down may be pessimistic, since photon noise component may be too large. The

altitudes z are actually the detector footprints of the linear detector array projected to the Earth limb. The w_{vi} as defined above weight channels with least variance summed over all altitudes the most.

An iterative solution for (A8) for the species modification coefficients $a_{z'i}$ that resembles the Newtonian iterative approach (i.e., resembles equation (99) in the *Rodgers* [1976] paper) is given by the equation

$$(\mathbf{a}_i - \mathbf{I}) = \mathbf{f}_{vi}^{-1}[\mathbf{k}_i\mathbf{S}_{\varepsilon i}^{-1}(\mathbf{b}_i - \mathbf{I}) + \mathbf{S}_x^{-1}(\mathbf{\Lambda}_i - \mathbf{I})] \quad \text{(A9)}$$

where $\mathbf{a}_i$ is the vector form of a_{zi} with elements at z, likewise $\mathbf{b}_i$ is the vector form of b_{zi} with elements at z. The quantity $\mathbf{S}_{\varepsilon i}$ is a diagnol instrument noise matrix with elements that are related to the noise to signal ratio at z for species i. The smoothing matrix $\mathbf{S}_x$ functions much like the solution covariance matrix of the Newtonian iterative method. To provide a smooth transition from the data-driven retrieval to an a priori solution X_{zi}^A on going from regions where the signal to noise is more than unity to regions where the signal to noise is less than unity, the matrix $\mathbf{S}_x$ may be given by

$$S_{xzz'} = 1 \quad \text{for} \quad z = z'$$

$$S_{xzz'} = 0 \quad \text{for} \quad z \neq z'. \quad \text{(A10)}$$

The inverse of the fractional variance matrix $\mathbf{f}_{vi}$ is defined by

$$\mathbf{f}_{vi} = (\mathbf{S}_x^{-1} + \mathbf{k}_i^T\mathbf{S}_{\varepsilon i}^{-1}\mathbf{k}_i) \quad \text{(A11)}$$

and the diagnol elements of $\mathbf{f}_{vi}^{-1}$ are the fractional variances of the solution a_{zi}. By the definition (equation (A10)) of the smoothing matrix $\mathbf{S}_x$ the fractional variance of the solution $\mathbf{f}_{vi}^{-1}$ goes to 1 as signal to noise goes to zero.

On implementing (A9), the a priori solution is related to the nth trial solution by the relation $X_{zi}^A = A_{zi}X_{zi}^{(n)}$. The vector form of the A_{zi} is $\mathbf{A}_i$. The matrix $\mathbf{I}$ is the unit matrix.

A5. Embedded Production Data Error Estimates

By the method above, the fractional error estimates E_{fzi} at altitude z are given by

$$E_{\text{fzi}} = (f_{vizz}^{-1})^{1/2} \quad \text{(A12)}$$

The values obtained for E_{fzi} are driven by what is selected for the elements of $\mathbf{S}_{\varepsilon i}$. In V7 these elements are given by

$$S_{\varepsilon izz}^{-1} = (\text{b}_{zi}/\sigma_{\text{bzi}})^2 \quad \text{(A13)}$$

A potential problem with this approach is that sometimes, due to systematic effects, the quantity $b_{zi}/\sigma_{\text{bzi}}$ will be smaller than one would expect for random noise. Systematic effects such as poor knowledge of spectral parameters, or of the spectral characteristics of the instrument, or both, can introduce a systematic component to the reported error bars. Unfiltered noise spikes will also result in error bars that are larger than would be the case for pure random noise.

From the discussion above, it is clear that E_{fzi} is confined to the range $0 \leq E_{\text{fzi}} \leq 1.0$. Standard definition for the UARS error bars is not fractional error E_{fzi} but instead is actual error E_{azi} in units of volume mixing ratio. The simple presentation of $E_{\text{azi}} = E_{\text{fzi}}X_{zi}$ works very well for $E_{\text{fzi}} \ll 1$ but might be misleading for values of E_{fzi} approaching 1.0 since in this case the maximum attainable fractional error might be mistaken for a factor of 2 uncertainty on the upper limiting value. To attempt to avoid this situation the CLAES error bar E_{azi} for V7 data X_{zi} on the Eos DAAC is given as a function of the fractional error E_{fzi} as follows:

$$E_{\text{azi}} = X_{zi}(E_{\text{fzi}} + E_{\text{fzi}}/(1 - E_{\text{fzi}}))/2 \quad \text{(A14)}$$

In this form, $E_{\text{azi}} = E_{\text{fzi}}X_{zi}$ for small E_{fzi} as expected, but the maximum attainable fractional error 1.0 would not be inadvertantly mistaken for a factor of 2 uncertainty. The approach for going from E_{fzi} to E_{azi} as described may not be optimal, but it is what is done in producing the error bars for the CLAES V7. It is subject to modification in future versions.

A6. Mistakes in Embedded CLAES V7 Production Data Error Estimates

Because of conceptual errors the CLAES V7 production code did not exactly follow the error estimation algorithm described above. This led to an overestimate of CLAES error by no more than 15% for all CLAES species other than ozone retrieved from blocker region 9, i.e., the CLAES O_3B9 subtype. For O_3B9 the error was exacerbated to the extent that the fractional error could be a factor $\approx(6.1)^{1/2}$ larger than it should be in regions where there is significant signal to noise. However, it still tends to go to 1 in regions of zero signal to noise.

The reason is twofold. First, in the V7 code the fractional variances of the solution a_{zi} were computed by $(S_{xzz}^{-1}/f_{\text{vizz}})^{1/2}$ rather than by (A12) above. This would not affect the numerical value except that the second error is that the smoothing matrix in the V7 code was mistakenly given nonzero off diagnol elements. For O_3B9 these were $e^{-n/5}$ where n tells how far off diagnol the element is. In this case the diagnol element of the inverse of the smoothing matrix $S_{xzz}^{-1} \approx 6.1$. Thus in the case of very small signal to noise the fractional variance goes to 1 as it should, but for large signal to noise, the fractional variance becomes $\approx(6.1)^{1/2}$ larger than it should. This discrepancy between the V7 production error bars and estimates derived from other sources is quite clear, as is discussed by *Bailey et al.* [this issue].

For all subtypes other than O_3B9 the V7 off diagnol smoothing matrix elements were e^{-n}. Therefore the maximum value of the diagnol element of the inverse of the smoothing matrix $S_{xzz}^{-1} \approx 1.3$. In this case, the maximum overestimate in the V7 error bars was at most 15% in regions of large signal to noise.

Appendix B: Acronyms

AAOE	Airborne Antarctic Ozone Experiment.
AASE	Airborne Arctic Stratosphere Expedition.
AC	period averaged (many days) zonal mean HNO_3 column (molecules/cm^2).
ATMOS	Atmospheric Trace Molecule Spectroscopy (ATMOS) Experiment.
ATLAS	Atmospheric Laboratory for Applications and Science.
BLISS	balloon-borne laser in situ sensor.
CAESR	cold atmosphere emission spectral radiometer.
CLAES	cryogenic limb array etalon spectrometer.
CLAES V7	processed CLAES data version 7.
CLAES · $O_3C_{>100}$	CLAES column ozone above 100 mbar.
DCD	HNO_3 column data reported by *David et al.* [1994].
EGA	emissivity growth approximation.

FIRS-2	far-infrared spectrometer.
FTS	Fourier transform spectrometer.
HITRAN92	spectral parameters database [*Rothman et al.*, 1992].
ISAMS	improved stratospheric and mesospheric sounder.
JPL	Jet Propulsion Laboratory.
KCD	HNO_3 column data reported by *Koike et al.* [1994].
LAAM	limb acquisition and adjustment mirror.
LIMS	limb infrared monitor of the stratosphere.
LLNL	Lawrence Livermore National Laboratory.
MkIV	JPL Mark IV interferometer.
MIPAS-B	Michelson interferometer for passive atmospheric sounding, balloon-borne version.
MLP	period(s) appropriate for establishing deseasonalized trends from CLAES data obtained in the latitude range between 32°S and 32°N; see discussion in section 5.1.3.
MLS	microwave limb sounder.
MLS · $O_3C_{>100}$	MLS column ozone above 100 mbar.
NESR	noise equivalent spectral radiance.
NLP	north-looking period(s); see Table 6.
OBCS	onboard blackbody calibration source.
PRT	platinum resistance thermometer.
QBO	quasi-biennial oscillation.
rfPac	the mechanism: recovery from HNO_3 enhancement due to Pinatubo aerosol surface conversion of N_2O_5 to HNO_3.
RMS	root-mean-square, i.e., $((\Sigma_{i=1}^{I} x_i^2)/I)^{1/2}$.
RSS	root sum of squares, i.e., $(\Sigma_{i=1}^{I} x_i^2)^{1/2}$.
SAGE	Stratospheric Aerosol and Gas Experiment.
SLP	south-looking period(s); see Table 5.
SLS	sub-millimeter-wave limb sounder.
TOMS	total ozone mapping spectrometer.
UARS	Upper Atmosphere Research Satellite.
VC	variability in period averaged zonal mean HNO_3 column.
vmr	volume mixing ratio.

Acknowledgments. We thank our LPARL colleague Frank Zele for his contributions to the production of the figures presented in this paper. We thank Praful Bhatt at LaRC for providing LIMS zonal mean data for plotting. We thank Gretchen Lingenfelser and Bill Grose at LaRC for assistance in bringing together the comparison data and for initial analyses of some of these. We thank L. V. Lyjak and C. A. Craig of NCAR for assistance in producing repeatability error estimates and ATMOS comparisons, respectively. We thank S. J. David of Denver University for providing her data by e-mail. We especially thank the referees for stimulating comments and suggestions that considerably improved the quality and content of the paper. At LPARL this work was supported by the NASA UARS contract NAS5-27752, at NCAR by the NASA UARS contract S-10782-C, the FIRS-2, BLISS, SLS, MARK IV, CAESR, and Bomem FTS correlative measurements by the NASA UARS correlative program, and the ATMOS by personnel at the Jet Propulsion Laboratory, California Institute of Technology, under contract with the National Aeronautics and Space Administration.

References

Bailey, P. L., et al., A comparison of CLAES ozone observations with correlative measurements, *J. Geophys. Res.*, this issue.

Chipperfield, M. P., and L. J. Gray, Two-dimensional model studies of the interannual variability of trace gases in the middle atmosphere, *J. Geophys. Res.*, *97*, 5963–5980, 1992.

Chipperfield, M. P., L. J. Gray, J. S. Kinnerly, and J. Zawodny, A two-dimensional model study of the QBO signal in SAGE II NO_2 and O–3, *Geophys. Res. Lett.*, *21*(7), 589–592, 1994.

Clarmann, T. von, H. Fischer, F. Friedl-Vallon, A. Linden, H. Oelhaf, C. Piesch, M. Seefeldner, and W. Volker, Retrieval of stratospheric O_3, HNO_3, and $ClONO_2$ profiles from 1992 MIPAS-B limb emission spectra: Method, results, and error analysis, *J. Geophys. Res.*, *98*, 20,495, 1993.

Clarmann, T. von, H. Fischer, F. Friedl-Vallon, A. Linden, H. Oelhaf, C. Piesch, M. Seefeldner, and W. Volker, Retrieval of stratospheric O_3 HNO_3 and $ClONO_2$ profiles from 1992 MIPAS-B limb emission spectra: Method, results, and error analysis, *J. Geophys. Res.*, *98*, 20,495–20,506, 1994.

David, S. J., F. J. Murcray, A. Goldman, C. P. Rinsland, and D. G. Murcray, The effect of the Mt. Pinatubo aerosol on the HNO_3 column over Mauna Loa, Hawaii, *Geophys. Res. Lett.*, *21*(11), 1003–1006, 1994.

Evans, W. F. J., J. B. Kerr, D. J. Wardle, J. C. McConnell, B. A. Ridley, and H. I. Schiff, Intercomparison of NO, NO_2, and HNO_3 measurements with photo-chemical theory, *Atmosphere*, *14*, 189, 1976.

Farman, J. C., B. G. Gardiner, and J. D. Shanklin, Large losses of total ozone in Antarctica reveal seasonal ClO_x/NO_x interaction, *Nature*, *315*, 207–210, 1985.

Farmer, C. B., High resolution infrared spectroscopy of the sun and earth's atmosphere from space, *Mikrochem. Acta*, *3*, 189, 1987.

Farmer, C. B., O. F. Raper, and F. G. O'Callaghan, Final report on the first of the ATMOS instrument during the Spacelab 3 mission, April 29 through May 6, 1985, *JPL Publ. 87-32*, 45 pp., Jet Propul. Lab., Pasadena, Calif., Oct. 1, 1987.

Fontanella, J.-C., A. Girard, L. Gramount, and N. Louisnard, Vertical distribution of NO, NO_2 and HNO_3 as derived from stratospheric absorption infrared spectra, *Appl. Opt.*, *14*, 825, 1975.

Froidevaux, L., J. W. Waters, W. G. Read, L. S. Elson, D. A. Flower, and R. F. Jarnot, Global ozone observations from the UARS MLS: An overview of zonal-mean results, *J. Atmos. Sci.*, *51*(20), 2846–2866, 1994.

Gille, J. C., and J. M. Russell III, The limb infrared monitor of the stratosphere: Experiment description, performance, and results, *J. Geophys. Res.*, *89*, 5125–5140, 1984.

Gille, J. C., et al., Accuracy and precision of the nitric acid concentrations determined by the limb infrared monitor of the stratosphere experiment on Nimbus 7, *J. Geophys. Res.*, *89*, 5179–5190, 1984.

Gille, J. C., et al., Accuracy and precision of cryogenic limb array etalon spectrometer (CLAES) temperature retrievals, *J. Geophys. Res.*, this issue.

Giver, L. P., F. P. J. Valero, D. Goorvitch, and F. S. Bonomo, Nitric-acid band intensities and band-model parameters from 610 to 1760 cm^{-1}, *J. Opt. Soc. Am. B*, *1*, 712–722, 1984.

Goldman, A., and C. P. Rinsland, HNO_3 line parameters: New results and comparisons of simulations with high-resolution laboratory and atmospheric spectra, *J. Quant. Spectrosc. Radiat. Transfer*, *48*, 653–666, 1992.

Goldman, A., C. P. Rinsland, F. J. Murcray, R. D. Blatherwick, and D. G. Murcray, High resolution studies of heavy NO_y molecules in atmospheric spectra, *J. Quant. Spectrosc. Radiat. Transfer*, *52*, 367–377, 1994.

Gray, L. J., and S. Ruth, The interannual variability of trace gases in the stratosphere: A comparative study of the LIMS and UARS measurement periods, *Geophys. Res. Lett.*, *19*(7), 673–676, 1992.

Gunson, M. R., C. B. Farmer, R. H. Norton, R. Zander, C. P. Rinsland, J. H. Shaw, and B.-C. Gao, Measurements of CH_4, N_2O, CO, H_2O, and O_3 in the middle atmosphere by the atmospheric trace molecule spectroscopy experiment on Spacelab 3, *J. Geophys. Res.*, *95*, 13,867, 1990.

Hoffman, D. J., and S. Solomon, Ozone destruction through heterogeneous chemistry following the eruption of El Chicón, *J. Geophys. Res.*, *94*, 5029–5041, 1989.

James, T. C., A. E. Roche, and J. B. Kumer, Model calculations of spectral transmission for the CLAES etalons, in Proceedings of the

Society of Photo-Optical Instrumentation Engineers, *Proc. SPIE, 973*, 353, 1988.

Johnson, D. G., K. W. Jucks, W. A. Traub, and K. V. Chance, Smithsonian stratosphere far-infrared spectrometer and data reduction system, *J. Geophys. Res.*, in press, 1995.

Jones, N. B., M. Koike, W. A. Matthews, and B. M. McNamara, Southern hemisphere mid latitude seasonal cycle in total column nitric acid, *Geophys. Res. Lett.*, *21*(7), 593–596, 1994.

Koike, M., N. B. Jones, W. A. Matthews, P. V. Johnston, R. L. McKenzie, D. Kinnison, and J. Rodriguez, Impact of Pinatubo aerosols on the partitioning between NO_2 and HNO_3, *Geophys. Res. Lett.*, *21*(7), 597–600, 1994.

Kumer, J. B., and J. L. Mergenthaler, Pressure, temperature, and ozone profile retrieval from simulated atmospheric earthlimb infrared emission, *Appl. Opt.*, *30*(9), 1124–1131, 1991.

Kumer, J. B., J. L. Mergenthaler, T. C. James, A. E. Roche, L. W. Sterritt, and J. F. Potter, Detector channeling hypothesis for enhanced structure observed in CLAES system blocker filter functions, in *Optical Remote Sensing of the Atmosphere, Tech. Dig. Ser.*, vol. 4, *Pap. MD22*, p. 164, Opt. Soc. of Am., New York, 1990.

Kumer, J. B., J. L. Mergenthaler, and A. E. Roche, CLAES CH_4, N_2O and CF_2Cl_2 (F12) global data, *Geophys. Res. Lett.*, *20*(12), 1239–1242, 1993.

Lazrus, A. L., and B. W. Gandrud, Distribution of stratospheric nitric acid vapor, *J. Atmos. Sci.*, *31*, 1102, 1974.

Marshall, B. T., L. L. Gordley, and D. A. Chu, BANDPAK: Algorithms for modeling broadband transmittance and radiance, *J. Quant. Spectrosc. Radiat. Transfer*, *52*, 563–580, 1994.

Massie, S. T., et al., Validation studies using multiwavelength CLAES observations of stratospheric aerosol, *J. Geophys. Res.*, this issue.

Mergenthaler, J. L., J. F. Potter, J. B. Kumer, T. C. James, and A. E. Roche, Retrieval of CLAES Filter Shapes from spectral Calibration Data, in *Optical Remote Sensing of the Atmosphere, Tech. Dig. Ser.*, vol. 4, *Pap. MD26*, p. 180, Opt. Soc. of Am., New York, 1990.

Mergenthaler, J. L., J. B. Kumer, and A. E. Roche, CLAES south-looking aerosol observations for 1992, *Geophys. Res. Lett.*, *20*(12), 1295–1298, 1993.

Murcray, D. G., T. G. Kyle, F. H. Murcray, and W. J. Williams, Nitric acid and nitric oxide in the lower stratosphere, *Nature*, *218*, 78–79, 1968.

Murcray, D. G., D. D. Barker, J. N. Brooks, A. Goldman, and W. J. Williams, Seasonal and latitudinal variations of the stratospheric concentration of HNO_3, *Geophys. Res. Lett.*, *2*, 223, 1975.

Murcray, F. J., J. J. Kosters, R. D. Blatherwick, J. Olson, and D. G. Murcray, High resolution solar spectrometer system for measuring atmospheric constituents, *Appl. Opt.*, *29*, 1520–1525, 1990.

Murcray, F. J., J. R. Starkey, W. J. Williams, W. A. Matthews, U. Schmidt, P. Aimedieu, and C. Camy-Peyret, HNO_3 profiles obtained during the EASOE campaign, *Geophys. Res. Lett.*, *21*, 1223, 1994.

Reber, C. A., The Upper Atmosphere Research Satellite (UARS), *Geophys. Res. Lett.*, *20*, 1215–1218, 1993.

Rinsland, C. P., M. R. Gunson, M. C. Abrams, L. L. Lowes, R. Zander, E. Mahieu, A. Goldman, M. K. W. Ko, J. M. Rodriguez, and N. D. Sze, Heterogeneous conversion of N_2O_5 to HNO_3 in the post-Mount Pinatubo eruption stratosphere, *J. Geophys. Res.*, *99*, 8213–8219, 1994.

Roche, A. E., J. B. Kumer, J. L. Mergenthaler, G. A. Ely, W. G. Uplinger, J. F. Potter, T. C. James, and L. W. Sterritt, The cryogenic limb array etalon spectrometer (CLAES) on UARS: Experiment description and performance, *J. Geophys. Res.*, *98*, 10,763–10,775, 1993a.

Roche, A. E., J. B. Kumer, and J. L. Mergenthaler, CLAES Observations of $ClONO_2$ and HNO_3 in the Antarctic stratosphere, between June 15 and September 17, 1992, *Geophys. Res. Lett.*, *20*, 1223–1226, 1993b.

Roche, A. E., J. B. Kumer, and J. L. Mergenthaler, R. W. Nightingale, W. G. Uplinger, G. A. Ely, J. F. Potter, D. J. Wueblles, P. S. Connell, and D. E. Kinnison, Observations of lower stratospheric $ClONO_2$, HNO_3 and aerosol by the UARS CLAES experiment between January 1992 and April 1993, *J. Atmos. Sci.*, *51*(20), 2877–2902, 1994.

Rodgers, C., Retrieval of atmospheric temperature and composition from remote measurements of thermal radiation, *Rev. Geophys.*, *14*, 609–624, 1976.

Rodgers, C. D., R. J. Wells, R. G. Grainger, and F. W. Taylor, Improved stratospheric and mesospheric sounder validation: General approach and in-flight radiometric calibration, *J. Geophys. Res.*, this issue.

Rodriguez, J. M., Probing stratospheric ozone, *Science*, *261*, 1128–1129, 1993.

Rothman, L. S., et al., The HITRAN molecular database: Editions of 1991 and 1992, *J. Quant. Spectrosc. Radiat. Transfer*, *48*, 469–507, 1992.

Russell, J. M., III, C. B. Farmer, C. P. Rinsland, R. Zander, L. Froidevaux, G. C. Toon, B. Gao, J. Shaw, and M. R. Gunson, Measurements of odd nitrogen compounds in the stratosphere by the ATMOS experiment on Spacelab 3, *J. Geophys. Res.*, *93*, 1718–1736, 1988.

Santee, M. L., W. G. Read, J. W. Waters, L. Froidevaux, G. L. Manney, D. A. Flower, R. F. Jarnot, R. S. Harwood, and G. E. Peckham, Interhemispheric differences in polar stratospheric HNO_3, H_2O, ClO and O_3, *Science*, *267*, 849–852, 1995.

Spreng, S., and F. Arnold, Balloon-borne mass spectrometer measurements of HNO_3 and HCN in the winter Arctic stratosphere—Evidence for HNO_3-processing by aerosols, *Geophys. Res. Lett.*, *21*(13), 1251, 1994.

Stachnik, R. A., J. C. Hardy, J. A. Tarsala, J. W. Waters, and N. R. Erickson, Submillimeterwave heterodyne measurements of stratospheric ClO, HCl, O_3, and HO_2: First results, *Geophys. Res. Lett.*, *19*, 1931, 1992.

Sterritt, L. W., T. C. James, J. B. Kumer, A. E. Roche, B. C. Steakley, and K. M. Zickuhr, Cryogenic limb array etalon spectrometer (CLAES) calibration, in *Cryogenic Optical Systems and Instruments*, vol. IV, *Proc. SPIE*, *1340*, 194, 1990.

Taylor, F. W., et al., Remote sensing of atmospheric structure and composition by pressure modulator radiometry from space: The ISAMS experiment on UARS, *J. Geophys. Res.*, *98*, 10,799–10,814, 1993.

Toon, G. C., JPL Mark IV interferometer, *Opt. Photonics News*, *2*, 19–21, 1991.

Traub, W. A., K. V. Chance, D. G. Johnson, and K. W. Jucks, Stratospheric spectroscopy with the far-infrared spectrometer (FIRS-2): Overview and recent results, *Proc. SPIE*, *1491*, 298, 1991.

Traub, W. A., K. W. Jucks, D. G. Johnson, M. T. Coffey, W. G. Mankin, and G. C. Toon, Comparison of column abundances from three infrared spectrometers during AASE II, *Geophys. Res. Lett.*, *21*(23), 2591–2594, 1994a.

Traub, W. A., K. W. Jucks, D. G. Johnson, and K. V. Chance, Chemical change in the Arctic vortex during AASE II, *Geophys. Res. Lett.*, *21*(23), 2595–2598, 1994b.

Tuck, A. F., R. T. Watson, E. P. Condon, J. J. Margitan, and O. B. Toon, The planning and execution of ER-2 and DC-8 aircraft flights over Antarctica, August and September 1987, *J. Geophys. Res.*, *94*, 11,181–11,222, 1989.

Turco, R., A. Plumb, and E. Condon, The Airborne Arctic Stratosphere Expedition: Prologue, *Geophys. Res. Lett.*, *17*, 313–316, 1990.

Waters, J. W., Microwave limb sounding, *Atmospheric Remote Sensing by Microwave Radiometry*, John Wiley, New York, 1993.

Webster, C. R., and R. D. May, Simultaneous in situ measurements and diurnal variations of NO, NO_2, O_3, NO_2, CH_4, H_2O, and CO_2 in the 40- to 26-km region using an open path tunable diode laser spectrometer, *J. Geophys. Res.*, *92*, 11,931, 1987.

Webster, C. R., R. D. May, R. Toumi, and J. A. Pyle, Active nitrogen partitioning and the nighttime formation of N_2O_5 in the stratosphere: Simultaneous in situ measurements of NO, NO_2, HNO_3, O_3, and N_2O using the BLISS diode laser spectrometer, *J. Geophys. Res.*, *95*, 13,851, 1990.

Webster, C. R., R. D. May, M. Allen, and L. Jaegle, *Geophys. Res. Lett.*, *21*, 53–56, 1994.

M. C. Abrams, J.-F. Blavier, M. R. Gunson, R. D. May, B. Sen, R. A. Stachnik, and C. R. Webster, Jet Propulsion Laboratory, Pasadena, CA 91109.

P. L. Bailey, J. C. Gille, and S. T. Massie, National Center for Atmospheric Research, P. O. Box 3000, Boulder, CO 80307.

G. A. Ely, J. B. Kumer (corresponding author), J. L. Mergenthaler, R. W. Nightingale, A. E. Roche, and W. G. Uplinger, Lockheed Palo Alto Research Laboratory, 3521 Hanover Street, Palo Alto, CA 94304.

A. Goldman, D. G. Murcray, and F. J. Murcray, University of Denver, Denver, CO 80210.

D. G. Johnson, K. W. Jucks, and W. A. Traub, Smithsonian Astrophysical Observatory, Cambridge, MA 02138.

(Received March 4, 1995; revised November 18, 1995;
accepted November 18, 1995.)